# Light neutral *CP*-even Higgs boson within the next-to-minimal supersymmetric standard model at the Large Hadron Electron Collider

Siba Prasad Das[1,*] and Marek Nowakowski[1,2,†]

[1]*Department of Physics, Faculty of Science, Universidad de los Andes,*
*Apartado Aereo 4976-12340, Carrera 1 18A-10, Bogota, Colombia*
[2]*M. Smoluchowski Institute of Physics, Jagiellonian University,*
*ul. St. Lojasiewicza 11, 30-348 Kraków, Poland*

We analyze the prospects of observing the light charge parity (*CP*)-even neutral Higgs bosons ($h_1$) in their decays into $b\bar{b}$ quarks, in the neutral and charged current production processes $eh_1q$ and $\nu h_1q$ at the upcoming Large Hadron Electron Collider (LHeC), with $\sqrt{s} \approx 1.296$ TeV. Assuming that the intermediate Higgs boson ($h_2$) is Standard Model (SM)-like, we study the Higgs production within the framework of next-to-minimal supersymmetric Standard Model (NMSSM). We consider the constraints from dark-matter, sparticle masses, and the Higgs boson data. The signal in our analysis can be classified as three jets, with electron (missing energy) coming from the neutral (charged) current interaction. We demand that the number of $b$-tagged jets in the central rapidity region be greater or equal to two. The remaining jet is tagged in the forward regions. With this forward jet and two $b$-tagged jets in the central region, we reconstructed three jets invariant masses. Applying some lower limits on these invariant masses turns out to be an essential criterion to enhance the signal–to–background rates, with slightly different sets of kinematical selections in the two different channels. We consider almost all reducible and irreducible SM background processes. We find that the non-SM like Higgs boson, $h_1$, would be accessible in some of the NMSSM benchmark points, at approximately the $0.4\sigma$ ($2.5\sigma$) level in the $e + 3j$ channel up to Higgs boson masses of 75 GeV, and in the $\not{E}_T + 3j$ channel could be discovered with the $1.7\sigma$ ($2.4\sigma$) level up to Higgs boson masses of 88 GeV with 100 fb$^{-1}$ of data in a simple cut-based (with optimization) selection. With ten times more data accumulation at the end of the LHeC run, and using optimization, one can have $5\sigma$ discovery in the electron (missing energy) channel up to 85 (more than 90) GeV.

## I. INTRODUCTION

It has long been expected that the mechanism that triggers the electroweak symmetry breaking (EWSB) and generates the fundamental particle masses will involve at least two experimental parts. The first one is the search and the observation of a spin-zero Higgs particle that will confirm the scenario of the minimal Standard Model (SM) (which has one Higgs isospin doublet) of Glashow-Weinberg-Salam and most of its extensions. This confirms a spontaneous symmetry breaking by a scalar field that develops a nonzero vacuum expectation value (vev). This part has recently been closed by the ATLAS and CMS experiments [1,2] at the Large Hadron Collider (LHC) with the spectacular observation of a new boson with a present central mass value around $125.09 \pm 0.21 \pm 0.11$ GeV. The width, and the couplings to all SM particles and the charge parity (*CP*)-quantum numbers are also known. All this seems consistent with the symmetry breaking mechanism in the SM and opens up the second part: are there any other scalars from beyond the SM, which would participate in the

symmetry breaking? This second part is mandatory in order to establish the exact nature of the electroweak symmetry breaking (EWSB) mechanism and, eventually, identify the effects of new physics beyond the SM.

The original idea of having scalars in the model is, of course, the spontaneous breaking of the electroweak gauge group. A detailed overview has been given in [3] and in particular the nonstandard way of the EWSB in [4]. However, scenarios where the scalars do not participate in the EWSB do exist (see, for instance, neutrino models where the vevs of singlet scalars spontaneously break the lepton number [5]).

Also worth mentioning are the higher dimensional theories, based on the Standard Model gauge group [6] where the electroweak constraints can be consistent with experimental results, even without the Higgs boson. In this kind of model, the electroweak symmetry is broken by the boundary conditions and the choices of compactification scales lead to the masses of the gauge bosons.

The available theoretical models at our disposal are many: the generic two-Higgs doublet model (2HDM) [7,8] and various flavor-violating Yukawa-textured models [9], minimal supersymmetric Standard Model (MSSM) [10], nonminimal realization of supersymmetric models, and

*sp.das@uniandes.edu.co
†mnowakos@uniandes.edu.co

models with additional singlets, the next-to-minimal super-symmetric Standard Model (NMSSM), doublets and/or triplets [11–15] and the nonminimal NMSSM type of models, e.g., in [16,17]. Hence, one of the most important tasks for experimentalists and theorists is to find ways to either exclude or confirm aspects of these models which may have varieties of signatures for the different Higgs production and decay channels at the present and the upcoming collider experiments.

From the perspective of model building, the NMSSM [11–15] is ideally suited to search for new physics, as its gauge group is the same as in the SM, and thus it can easily accommodate the SM-like discovery without any unnatural fine-tuning of its parameters. Although the MSSM contains fewer free parameters than the NMSSM, the SM Higgs boson type signal can also be easily accommodated in the latter model, whereas some amount of fine-tuning is necessary for the MSSM. Some variants of the NMSSM models also have the nice features of the Higgs sector. Worth mentioning is the model with a slightly broken Peccei-Quinn (PQ)-symmetry [18] and the so-called $\lambda$-NMSSM [19].

It is worth pointing out that in the NMSSM the upper limit of the lightest SM-like Higgs boson mass is lifted up to 155 GeV (as compared to 139 GeV in the MSSM). Secondly, the problem with the absence of sparticle signals may easily be explained by different supersymmetry (SUSY) cascade decays occurring in the NMSSM, owing to an additional singlino entering as the last step and thereby inducing topologies to which present SUSY searches are less sensible. Furthermore, as is well known, the MSSM suffers from the so-called $\mu$-problem: i.e., the Higgs(ino) mass term entering the soft SUSY Lagrangian ought to be manually set at the EW scale in order to achieve EWSB, while SUSY itself would require it to be at the Planck scale (or else be zero, in virtue of some theoretical additional symmetry) [20,21]. This is elegantly remedied in the NMSSM, since herein the aforementioned soft term is replaced by the vev of an additional Higgs singlet state, which appears naturally at the EW scale. In turn, this implies that the Higgs sector of the NMSSM is very rich. In fact, while only one Higgs boson exists in the SM and five Higgs bosons exist in the MSSM, there are seven such states in the NMSSM: three $CP$-even Higgses $h_{1,2,3}$ ($m_{h_1} < m_{h_2} < m_{h_3}$), two $CP$-odd Higgses $a_{1,2}$ ($m_{a_1} < m_{a_2}$) and two charged Higgses $h^{\pm}$.

As the SM is embedded within any two-Higgs doublet model, the recently discovered SM-Higgs boson can be part of the spectrum. Generically, this SM-type Higgs is either the lightest $CP$-even neutral one or the second-lightest one. Light as well as heavy Higgs boson phenomenology within the MSSM has been studied extensively in [22]. Having many free parameters in NMSSM, the masses of the Higgs bosons vary in a wide range so that their decay branching ratios in various modes can also vary widely. The Higgs

boson masses together with their couplings to gauge boson and/or fermions are most important to identify the viable modes to look for the Higgs boson in any collider experiment. From the theoretical perspective, the two-loop corrected Higgs boson masses and couplings to quarks and gauge bosons within NMSSM have been carried out in [23,24].

The NMSSM Higgs boson phenomenology at high energy colliders has been studied over a decade [25–32] and direct experimental searches are reported in [33].

From the upcoming experiment perspective, the Large Hadron Electron Collider (LHeC) facility [34] is expected to be operational at CERN around 2020. It will be a deep inelastic scattering (DIS) experiment at the TeV scale, with the center-of-mass energy of around 1.3 TeV. In comparison, another recently closed (in 2007) DIS experiment [the Hadron-Electron Ring Accelerator (HERA) [35] at Deutsches Elektronen-Synchrotron (DESY) had a center-of-mass energy of around 320 GeV with an integrated luminosity of around 0.5 fb$^{-1}$]. The LHeC might deliver data samples of approximately 100 fb$^{-1}$ and at the end of full data accumulation with 1000 fb$^{-1}$ (with a higher detector coverage). Taking into consideration all kinematical and detector aspect details, the overall kinematic range (in $x$ and $Q^2$) at LHeC is 20 times larger than the HERA experiment. Other than the in-depth studies of QCD, the LHeC also has an enormous scope to probe electroweak and Higgs boson physics [36–38].

One of the nicest features of almost all SUSY models, is that the neutral lightest sparticle state is naturally the dark matter candidate [39,40]. Within the standard cosmological scenario, we assumed that the dark matter candidate is the lightest neutralino, $\tilde{\chi}_1^0$, with the correct abundance of relic density consistent with recent Planck measurement [41]. We refer to [42,43] where the dark matter phenomenology within NMSSM has been studied. Some variant models are discussed in [44], and a discussion on low mass weakly interacting massive particle (WIMP) searches consistent with the Higgs boson data at LHC has been studied recently in [45]. Sparticle co-annihilation consistent with the dark matter relic density and related SUSY phenomenology in the electroweak gaugino sector are discussed in [46,47].

To the best of our knowledge no study has been done to find non-SM type Higgs boson signals within the NMSSM at the LHeC. In our analysis, we assumed the second intermediate Higgs boson is the SM-type ($h_2$-SM scenario). This, of course, refers to the mass, coupling ratios and signal-strength from the recent LHC results. The lightest non-SM Higgs boson, $h_1$, offers itself to be looked for at the upcoming LHeC. We identify two main production processes, namely the neutral current one $ep \rightarrow eh_1 q$ and the charged current one $ep \rightarrow \nu h_1 q$. We are particularly motivated by the possible branching ratio enhancement in the $b$-quark decay mode, i.e., $h_1 \rightarrow b\bar{b}$. Finally the reconstructed invariant mass of the two $b$-tagged jets ensures the evidence of the non-SM-like Higgs boson.

The plan of this paper is as follows. In the next section we will briefly describe the NMSSM model. In Sec. II, we will randomly vary the NMSSM model parameters and identify the allowed parameter space consistent with the most up-to-date theoretical, phenomenological and experimental constraints. For the allowed model space, we then estimate the number of non-SM type Higgs boson signal events, $ep \to eh_1 q$ and $ep \to \nu h_1 q$ with the decay channel $h_1 \to b\bar{b}$ and identify a few high event-rated benchmark points to carry out the phenomenological analysis in Sec. III. In doing so, we estimate all the reducible and irreducible SM backgrounds for both of the signal channels under consideration. In Sec. IV, we carry out a simple cut-based optimization to isolate the Higgs boson signals in both the channels. We summarize our findings in Sec. V.

## II. THE NMSSM MODELS

The NMSSM model has been described in many reviews [11–15]. However, for completeness, let us mention the part relevant for our analysis (we will follow [15]).

The general NMSSM contains the MSSM superfields with most general renormalizable couplings as in the MSSM superpotential. There is, however, one additional gauge singlet chiral superfield $\hat{S}$.

The Higgs superpotential $W_{\text{Higgs}}$ reads

$$W_{\text{Higgs}} = (\mu + \lambda\hat{S})\hat{H}_u \cdot \hat{H}_d + \xi_F\hat{S} + \frac{1}{2}\mu'\hat{S}^2 + \frac{\kappa}{3}\hat{S}^3, \quad (1)$$

where $\lambda$, $\kappa$ are dimensionless Yukawa couplings. The bilinear $\mu$, $\mu'$ terms are the supersymmetric mass terms, and $\xi_F$ with mass-dimension two is the supersymmetric tadpole term.

Assuming R-parity and *CP*-conservation (scenarios without these requirements have been studied in [24,48]) the corresponding soft supersymmetry breaking terms, $\mathcal{L}_{\text{soft}}$ are the following:

$$-\mathcal{L}_{\text{soft}} = m^2_{H_u}|H_u|^2 + m^2_{H_d}|H_d|^2 + m^2_S|S|^2 + m^2_Q|Q^2| + m^2_U|U^2_R| + m^2_D|D^2_R| + m^2_L|L^2| + m^2_E|E^2_R|$$

$$+ \left( h_u A_u Q \cdot H_u U^c_R - h_d A_d Q \cdot H_d D^c_R - h_e A_e L \cdot H_d E^c_R \right.$$

$$\left. + \lambda A_\lambda H_u \cdot H_d S + \frac{1}{3}\kappa A_\kappa S^3 + m^2_3 H_u \cdot H_d + \frac{1}{2}m'^2_S S^2 + \xi_S S + \text{H.c.} \right), \quad (2)$$

where all the parameters have the standard meanings.

The dimensional supersymmetric parameters $\mu$, $\mu'$, and $\xi_F$ (with mass dimension two) in the superpotential, and the associated soft SUSY breaking parameters $m^2_3$, $m'^2_S$, and $\xi_S$ (with mass dimension three) have to be of the order of the weak or SUSY breaking scale.

In general, these terms are nonvanishing; however, a simplified version requiring scale invariance leads to $\mu = \mu' = \xi_F = 0$ and the superpotential takes the simple form

$$W_{\text{scale-invariant}} = \lambda\hat{S}\hat{H}_u \cdot \hat{H}_d + \frac{\kappa}{3}\hat{S}^3 \quad (3)$$

together with the parameters $m^2_3$, $m'^2_S$, and $\xi_S$ in (2) also set to zero. An effective $\mu$-term of the order of weak scale is generated from the vev $s$ of $\hat{S}$:

$$\mu_{\text{eff}} = \lambda s. \quad (4)$$

From the supersymmetric gauge interactions, the $F$-term and the soft supersymmetry breaking terms one can obtain the Higgs potential:

$$V_{\text{Higgs}} = |\lambda(H^+_u H^-_d - H^0_u H^0_d) + \kappa S^2 + \mu'S + \xi_F|^2 + (m^2_{H_u} + |\mu + \lambda S|^2)(|H^0_u|^2 + |H^+_u|^2)$$

$$+ (m^2_{H_d} + |\mu + \lambda S|^2)(|H^0_d|^2 + |H^-_d|^2) + \frac{g^2_1 + g^2_2}{8}(|H^0_u|^2 + |H^+_u|^2 - |H^0_d|^2 - |H^-_d|^2)^2 + \frac{g^2_2}{2}|H^+_u H^{0*}_d + H^0_u H^{-*}_d|^2$$

$$+ m^2_S|S|^2 + \left( \lambda A_\lambda(H^+_u H^-_d - H^0_u H^0_d)S + \frac{1}{3}\kappa A_\kappa S^3 + m^2_3(H^+_u H^-_d - H^0_u H^0_d) + \frac{1}{2}m'^2_S S^2 + \xi_S S + \text{H.c.} \right), \quad (5)$$

where $g_1$ and $g_2$ are $U(1)_Y$ and $SU(2)$ gauge couplings, respectively.

The physical neutral Higgs fields (with index R for the *CP*-even and index I for the *CP*-odd states) are obtained by expanding the full scalar potential (5) around the real neutral vevs $v_u$, $v_d$, and $s$:

$$H_u^0 = v_u + \frac{H_{uR} + iH_{uI}}{\sqrt{2}}, \qquad H_d^0 = v_d + \frac{H_{dR} + iH_{dI}}{\sqrt{2}},$$

$$S = s + \frac{S_R + iS_I}{\sqrt{2}}, \qquad (6)$$

where the vevs have to be obtained from the minima of

$$V_{\text{Higgs}} = (-\lambda v_u v_d + \kappa s^2 + \mu' s + \xi_F)^2 + \frac{g_1^2 + g_2^2}{8}(v_u^2 - v_d^2)^2$$
$$+ (m_{H_u}^2 + (\mu + \lambda s)^2)v_u^2 + (m_{H_d}^2 + (\mu + \lambda s)^2)v_d^2$$
$$+ m_S^2 s^2 - 2\lambda A_\lambda v_u v_d s + \frac{2}{3}\kappa A_\kappa s^3 - 2m_3^2 v_u v_d$$
$$+ m_S'^2 s^2 + 2\xi_S s. \qquad (7)$$

The minimization of (7) with respect the three vevs and the proper electroweak symmetry breaking (generating the correct Z-boson mass) leads to the following input parameters:

$$\lambda, \quad \kappa, \quad A_\lambda, \quad A_\kappa, \quad \tan\beta, \quad \mu_{\text{eff}}, \qquad (8)$$

to which one has to add the (in the convention $\mu = 0$) five parameters of the NMSSM:

$$m_3^2, \quad \mu', \quad m_S'^2, \quad \xi_F \quad \text{and} \quad \xi_S. \qquad (9)$$

The tree level Higgs mass matrices are obtained by expanding the full scalar potential (5) around the real neutral vevs $v_u$, $v_d$, and $s$ as in (6). The elements of the $3 \times 3$ $CP$-even mass matrix $\mathcal{M}_S^2$ are conveniently written in the basis $(H_{dR}, H_{uR}, S_R)$ after the elimination of $m_{H_d}^2$, $m_{H_u}^2$, and $m_S^2$.

The basis for the elements of the $3 \times 3$ $CP$-odd mass matrix $\mathcal{M}_P'^2$ are $(H_{dI}, H_{uI}, S_I)$. Dropping the Goldstone mode, in the remaining $2 \times 2$ $CP$-odd mass matrices, one can use the doublet ($M_A$) and singlet component ($M_P$) mass parameters as inputs together with the $\mu_{\text{eff}}$.

Our model under consideration is not the $Z_3$ invariant NMSSM, but rather a general phenomenological NMSSM. However, by setting $m_3^2 = m_S'^2 = \xi_S = \mu = \mu' = \xi_F = 0$ in the general phenomenological NMSSM, one recovers the $Z_3$ invariant NMSSM.

## III. THE NMSSM PARAMETER SPACES

We used the package NMSSMTOOLS 5.0.1 [49] to obtain the sparticle spectrum, decay branching ratios, and various low energy observables.

We randomly scanned approximately $10^6$ points. The varied parameters and their ranges are[1] tabulated in Table I.

---

[1]All the masses and mass parameters in our analysis are in GeV.

TABLE I. The minimum and maximum values of varied NMSSM parameters. The following parameters remain fixed: $M_3 = 1800.0$ GeV (this allows the gluino mass $m_{\tilde{g}}$ to be above the mass limits from recent LHC-run2); $m_{\tilde{\ell}} = 300.0$ GeV (for all three generations as well as left and right state) and $A_\tau = A_e = A_\mu = 1500.0$ GeV. Here, $M_A$ ($M_P$) is the doublet (singlet) component of the $CP$-odd Higgs mass matrices.

| Parameters | Minimum | Maximum |
|---|---|---|
| $\lambda$ | 0.001 | 0.7 |
| $\kappa$ | 0.001 | 0.7 |
| $A_\lambda$ | 100.0 | 2500.0 |
| $A_\kappa$ | −2500.0 | 100.0 |
| $\tan\beta$ | 1.5 | 60.0 |
| $\mu_{\text{eff}}$ | 100.0 | 500.0 |
| $M_1$ | 50.0 | 400.0 |
| $M_2$ | 50.0 | 500.0 |
| $m_{\tilde{q}_L}$ | 300.0 | 1500.0 |
| $A_t = A_b$ | −4000.0 | 1000.0 |
| $M_A$ | 100.0 | 500.0 |
| $M_P$ | 100.0 | 3000.0 |

For each randomly generated parameter space, we invoke the following constraints:

*Perturbative bounds:* We first imposed, $\lambda^2 + \kappa^2 \lesssim (0.7)^2$ [50], and, if not satisfied, we discard the parameter space and generate the next random model space.

*Dark matter relic density:* We required that the lightest neutralino relic density will be: $0.107 < \Omega_{\tilde{\chi}_1^0}h^2 < 0.131$, consistent with the Planck measurement [41] within standard cosmology. The estimated relic density ($\Omega_{\tilde{\chi}_1^0}h^2$) as a function of the $m_{\tilde{\chi}_1^0}$ has been shown in the left panel of Fig. 1 with constraining only the upper limits, i.e., $\Omega_{\tilde{\chi}_1^0}h^2 < 0.131$. The green-marked points within the upper and lower strips are consistent with the direct-detection and indirect-detection bounds (in the legends termed as: "All-DM").

The NMSSMTOOLS 5.0.1 is interfaced with MICRO-MEGAS v4.3 [51,52] to estimate the observed dark matter relic density, their direct detection, and indirect detection limits. It is to be noted that the standard and nonstandard cosmological implication in the dark matter relic density has been analyzed within the NMSSM in [29,42,43].

*Higgs bounds:* We demand that the intermediate Higgs boson ($h_2$) should be SM-like, and its mass should be within the range of 125.09 GeV $< m_{h_2} <$ 128.09 GeV (taken into consideration the 3 GeV error in theoretical estimates). Its coupling ratios to other SM particles should also be consistent with the LHC-run1 ATLAS and CMS combined study [53,54]. The allowed coupling ratios and the signal strengths considered in our analysis have been tabulated in Table II. We have also taken the constraint on
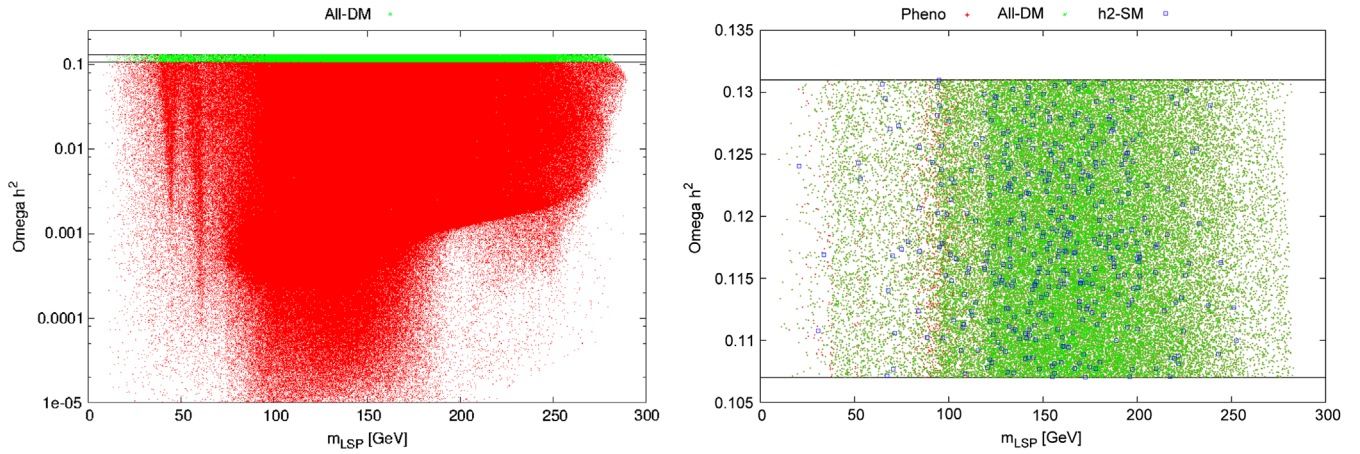
FIG. 1. Left panel: the dark matter relic density ($\Omega_{\tilde{\chi}_1^0} h^2$) as a function of the lightest neutralino masses ($m_{\tilde{\chi}_1^0}$) within the standard cosmology. The two lines represent the upper ($\Omega_{\tilde{\chi}_1^0} h^2 = 0.131$) and lower ($\Omega_{\tilde{\chi}_1^0} h^2 = 0.107$) bounds from the Planck measurements [41]. The first deep dip around 45 GeV is due to the Z-boson exchange (annihilation diagram) and the second around 63 GeV, from the Higgs-boson ($h_2$-SM) exchange annihilation within the NMSSM parameter spaces. The green points within the strips satisfy the direct and indirect dark matter search results and are termed as "All-DM". Right panel: we only show the relic density allowed parameter space together with various other constraints (in the legends), see the text for details.

the invisible branching ratio: $\mathrm{BR}(h_{\mathrm{SM}} \to invisible) \lesssim 0.25$ [55,56].[2] Furthermore, we required $m_{h^\pm} > 80.0$ GeV.

*LEP bounds:* Direct SUSY searches at the LEP have set bounds on superpartners; in particular, the lighter chargino should satisfy $m_{\tilde{\chi}_1^\pm} > 103.5$ GeV. The other one refers to the Z invisible width and should satisfy $\Gamma_Z^{\mathrm{inv}} < 2$ MeV at 95% C.L. [58]. When the decay channel into $\tilde{\chi}_1^0 \tilde{\chi}_1^0$ opens, this width may exceed the experimental value.[3]

*B-physics bounds:* The rare decays of $B$ meson, such as $B_s \to \mu^+ \mu^-$, $B^+ \to \tau^+ \nu$, and $B_s \to X_s \gamma$ lead to the flavor constraints. In our analysis, we set the recent experimental results at 95% C.L.: $1.7 \times 10^{-9} < \mathrm{BR}(B_s \to \mu^+ \mu^-) < 4.5 \times 10^{-9}$ [60], $0.85 \times 10^{-4} < \mathrm{BR}(B^+ \to \tau^+ \nu) < 2.89 \times 10^{-4}$ [61], and $2.99 \times 10^{-4} < \mathrm{BR}(B_s \to X_s \gamma) < 3.87 \times 10^{-4}$ [60].

*Sparticle masses:* We have set the following lower bounds from the superparticle masses following [62]: $m_{\tilde{g}} \gtrsim 1600.0$ GeV, $m_{\tilde{t}_1} \gtrsim 95.0$ GeV, $m_{\tilde{b}_1} \gtrsim 325.0$ GeV, $m_{\tilde{q}_L} \gtrsim 600.0$ GeV, $m_{\tilde{\ell}_L} \gtrsim 100.0$ GeV, $\tilde{m}_{\nu_L} \gtrsim 90.0$ GeV, and $m_{\tilde{\tau}_1} \gtrsim 87.0$ GeV.

If the randomly generated NMSSM model spaces satisfy all the above constraints, we consider them for further phenomenological studies. In the left panel of Fig. 1, we calculated $\Omega_{\tilde{\chi}_1^0} h^2$ using the MICROMEGAS as a function the

mass of the cold-dark matter candidate ($m_{\tilde{\chi}_1^0}$). All the points satisfy the upper bounds coming from the recent Planck measurements [41], and the upper and lower bounds are 0.131 and 0.107, respectively, referring to the standard cosmological scenario. Within this strips, the green points satisfy the direct and indirect dark matter searches which we term as "All-DM". The lightest neutralino annihilation would occur via the Z-boson exchange diagram—this shows a dip around the $M_Z/2$, i.e., 45 GeV. This annihilation rate would get enhanced via the SM-Higgs boson ($h_2$) exchange diagram and this leads to another dip around $m_{h_2}/2$, i.e., 63 GeV.

In the right panel of Fig. 1, we invoke the other constraints discussed above. If the constraints on the sparticles masses, B-physics, and other phenomenological limits are satisfied, we indicate it by "Pheno"; and if the $h_2$-SM type scenario is satisfied, we indicate it by "h2-SM". All the constraints are imposed cumulatively. Finally, the h2-SM model is interesting, *per se*, to look for as it is an unusual scenario.

In the left panel of Fig. 2, we displayed the singlino component of the lightest neutralino, i.e., $N_{15}$ as a function of $m_{\tilde{\chi}_1^0}$ with all the constraints mentioned in the legend. This shows that the lightest neutralinos with $m_{\tilde{\chi}_1^0} \gtrsim 80$ GeV are more favorable with the $h_2$-SM type scenario. It can be seen that the singlino domination would occur mostly between 25 GeV and 250 GeV, while nonsinglino type $\tilde{\chi}_1^0$ would also be possible (would go up to 1%), but the mass ranges are rather squeezed, ranging between 100–250 GeV.

In the right panel of Fig. 2, we showed the masses of all the Higgs bosons satisfying all constraints. It turns out that the heavy *CP*-odd Higgs boson mass (we showed it up to

---

[2]The SM-like Higgs boson invisible decay within the NMSSM has been studied recently in [57].

[3]A light Higgs would significantly affect the muon anomalous magnetic moment $a_\mu = (g_\mu - 2)/2$, whose most accurate measurement comes from the E821 experiment [59]. Having large theoretical uncertainties with the measurements, we have not considered this constraint in our numerical scan and subsequent analysis.

TABLE II. The couplings ($\kappa$) and signal strength ($\mu$) have been allowed within $2\sigma$ ranges (except $\kappa_W$) from the combined ATLAS and CMS measurements [54], following Table 17 (upper panel) and Table 8, respectively.

| Parameters | Minimum | Maximum | Parameters | Minimum | Maximum |
|---|---|---|---|---|---|
| $\kappa_W$ | 0.81 | 0.99 | $\mu^{\tau\tau}_{VBF}$ | 0.50 | 2.10 |
| $\kappa_t$ | 0.99 | 1.89 | $\mu^{\tau\tau}_{ggF}$ | −0.20 | 2.20 |
| $|\kappa_\gamma|$ | 0.72 | 1.10 | $\mu^{bb}_{VH}$ | 0.00 | 2.00 |
| $|\kappa_g|$ | 0.61 | 1.07 | $\mu^{bb}_{ttH}$ | −0.90 | 3.10 |
| $|\kappa_\tau|$ | 0.65 | 1.11 | $\mu^{WW}_{VBF}$ | 0.40 | 2.00 |
| $|\kappa_b|$ | 0.25 | 0.89 | $\mu^{ZZ}_{ggF}$ | 0.51 | 1.81 |
| $Br(h_{\rm SM} \to inv.)$ | | 0.25 | $\mu^{\gamma\gamma}_{VBF}$ | 0.30 | 2.30 |
| | | | $\mu^{\gamma\gamma}_{ggF}$ | 0.66 | 1.56 |

1600.0 GeV) is quite heavy, as it mainly depends upon the values of $M_P$.

In the left panel of Fig. 3 we showed all the Higgs boson masses as a function of $m_{a_1}$. However, in comparison to the right panel of Fig. 2, here we additionally imposed the "All-DM", "Pheno", and "h2-SM" criteria. These particular parameter spaces are of phenomenological interest. In the right panel of Fig. 3, we show the decay branching ratios of the non-SM type $h_1$ in the light flavor quark mode: $h_1 \to gg + c\bar{c} + s\bar{s}$, tau-lepton: $h_1 \to \tau\bar{\tau}$, $b$-quark: $h_1 \to b\bar{b}$, and the much suppressed two-photon decay: $h_1 \to \gamma\gamma$.

For all these points we estimated the event rates for the two signal processes under consideration. We will describe the details in the following section.

## IV. NUMERICAL ANALYSIS

In our analysis, we consider the $h_2$-SM scenario following Fig. 3, such that the non-SM-like $h_1$ is light enough to have some appreciable production rates at LHeC.

In this section, we first describe the two main different production mechanisms of Higgs bosons at the LHeC collider. These are the neutral- and charged-current production, which lead to the $e + 3j$ and $\not{E}_T + 3j$ signals, respectively. As a result, we will have two different sets of SM backgrounds, which we will address in the subsequent section.

### A. Higgs bosons signals

In our analysis, we consider the leading production processes via the neutral current as well as charged current. As we consider an $ep$-collision, the neutral (charged) current gives charged (neutral) lepton, electron (neutrino) in the final states. Generally, the charged current production cross sections are larger than the neutral currents as shown in Fig. 5, which is mainly due to the isospin couplings. The production processes of the Higgs bosons are: $eh_1q$

and $\nu_e h_1 q$,[4] where $q$ (or its charge-conjugated version) is the light parton, i.e., $u$, $d$, $s$, $c$ or $g$.

The Higgs boson production in our analysis is mainly dominated by the t-channel vector-boson fusion (VBF) processes.

The couplings (the neutral and charged gauge-boson fusion vertex) relevant at LHeC are the following:

$$g_{h_1ZZ} = \frac{g_1{}^2 + g_2{}^2}{\sqrt{2}}(v_d S_{11} + v_u S_{12}),$$

$$g_{h_1WW} = \frac{g_2{}^2}{\sqrt{2}}(v_d S_{11} + v_u S_{12}). \tag{10}$$

Here $S_{11}$ and $S_{12}$ are the mixing parameters in the singlet–doublet Higgs mixing matrices. The $v_u$ and $v_d$ are the up-type and down-type Higgs doublet vevs, and $g_1$ and $g_2$ are the $U(1)_Y$ and $SU(2)_L$ gauge couplings. We have plotted the allowed couplings, $g_{h_1WW}$, (using red color plus points) complying with all the constraints discussed earlier in Fig. 4 (see the caption for details). The green points in the top right corner are for $g_{h_2WW}$, and the masses and the corresponding coupling values are consistent with the coupling ratios for the $h_2$-SM scenario, following Table II.

It is to be noted that the same couplings given in Eq. (10) are also responsible for the Higgs boson production (t-channel VBF) at the large electron positron (LEP) and hadron colliders. We would like to estimate the event rates for this kind of signal at the LEP colliders and also at the hadron colliders, like the recently closed Tevatron and presently operating LHC.

We find that the exact signal hard processes at LHeC under consideration are not possible at LEP, Tevatron and LHC. However, we estimated the closest processes that we

---

[4]Please recall that we are working in the $h_2$-SM scenario. This is to say that the second $CP$-even Higgs boson is the SM-type consistent with all the couplings and observables and, in particular, compatible with the recent Higgs discovery at the LHC experiments.
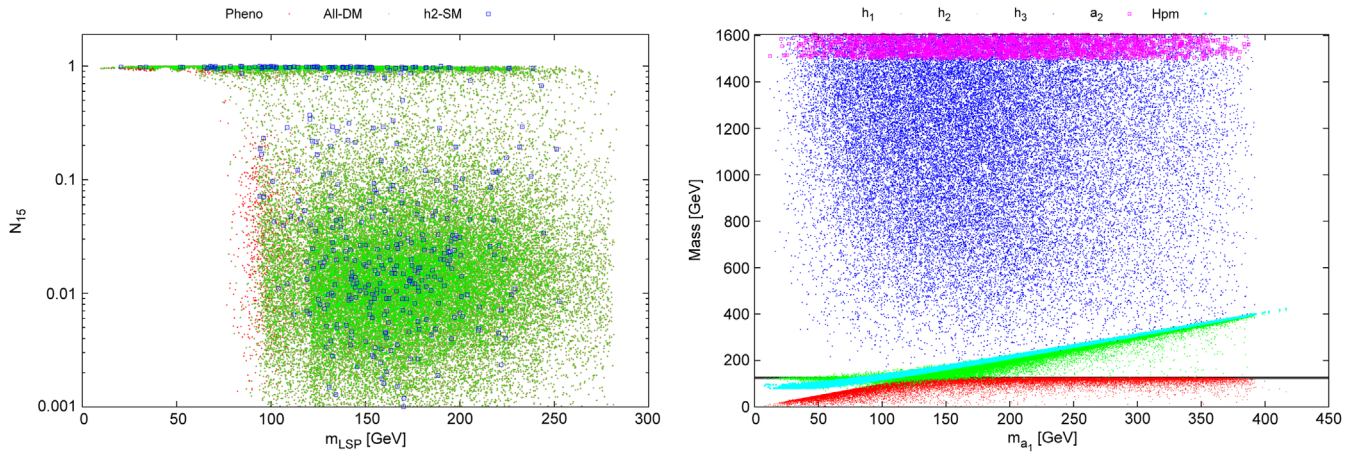
FIG. 2. Left panel: the singlet component ($N_{15}$) of the lightest neutralino ($\tilde{\chi}_1^0$) consistent with the dark matter relic density ($\Omega_{\tilde{\chi}_1^0} h^2$) and various other constraints (see text for details). Right panel: the masses of the Higgs boson masses, $h_1$, $h_2$, $h_3$, $a_2$, and $h^{\pm}$ ("Hpm") as a function of the lightest *CP*-odd Higgs boson masses ($m_{a_1}$). The mass of the $a_2$ is shown up to 1600.0 GeV and extends, however, even beyond this point in these allowed NMSSM model parameter spaces.
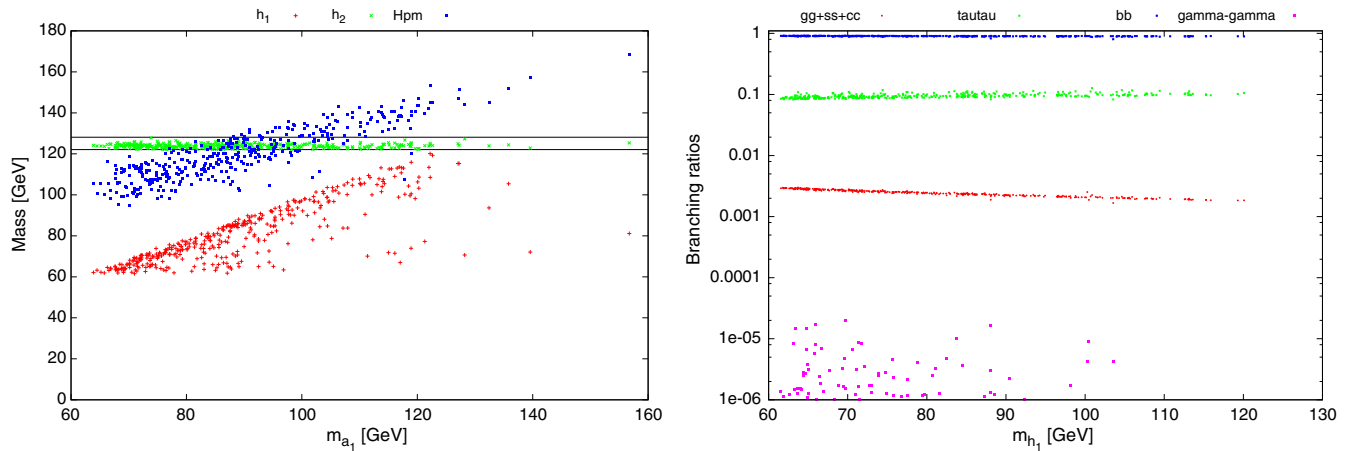


FIG. 3. Left panel: the Higgs boson masses, $h_1$, $h_2$, and $h^{\pm}$ as a function of the lightest *CP*-odd Higgs bosons mass ($m_{a_1}$) for the $h_2$-SM scenario and consistent with all other constraints (see details in the text). Right panel: we show the branching ratio of the $h_1$ in different channels, and it is clear that in the large region of allowed parameter space the branching ratio of $h_1 \to b\bar{b}$ is above 90%.

could have in these three colliders. At these colliders, we have estimated the event rates (in $fb$) with inclusion of Higgs branching ratios at the $e^+e^-$ LEP collider with center-of-mass energy 209 GeV, for the $\sigma(e^+e^- \to e^+ h_1 e^-)$ and $\sigma(e^+e^- \to \nu_e h_1 \bar{\nu}_e)$ processes in Fig. 6 in the left panel and right panel, respectively.

In hadron colliders, the closest process is $\sigma(pp, p\bar{p} \to jh_1 j)$, with $j = u, d, c, s, b, g$ and their charge conjugation. The estimated event rates (in $fb$) at Tevatron and LHC with center-of-mass energy 1.96 TeV and 14 TeV, is shown in Fig. 7, in the left panel and right panel, respectively. The LHC collider is presently operating and the number of events rates are substantial. In spite of the huge SM background contamination, it would be worth looking for this nonstandard Higgs signal in this ongoing machine.

We see from the right panel of Fig. 3 that $h_1$ is dominantly decaying into $b\bar{b}$. So our signals in both channels contain three jets (one is forward light flavored and two central b-tagged) and an electron (missing transverse energy) in case of neutral (charged) current.

We estimated the parton level signal cross sections using the MADGRAPH v 2.4.3 [63]. The allowed NMSSM model parameter spaces from the NMSSMTOOLS 5.0.1 [49] are written in SUSY Les Houches Accord (SLHA) format and fed to MADGRAPH v 2.4.3 [63]. The branching ratios (BRs) of the Higgs boson in all the decay modes is estimated by using NMHDECAY [49].

To obtain the cross sections at the LHeC [34,64–67], we consider an electron beam of energy $E_{e^-} = 60$ GeV, and a proton beam of energy $E_p = 7000$ GeV, corresponding to a center-of-mass energy of approximately $\sqrt{s} = 1.296$ TeV.
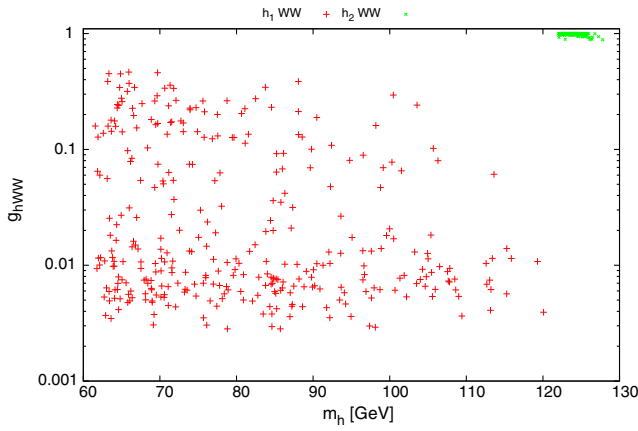
FIG. 4. The coupling $g_{hWW}$ (for $h = h_1$ and $h_2$) is shown as a function of the Higgs boson mass. The top right corner (with populated green points) shows the masses of the $h_2$ and the corresponding coupling constraints (that we imposed following Table II) from the recent LHC measurements.

To estimate the signal event rates at the parton level we applied the following basic preselections:

$$p_T^{q,e} > 10 \, \text{GeV}, \quad \eta^{q,e} < 5.0, \quad \Delta R(qq, qe) > 0.2, \quad (11)$$

with $\Delta R^2 = \Delta \eta^2 + \Delta \phi^2$, where $\eta$ and $\phi$ are the pseudorapidity and azimuthal angle, respectively. We take $m_t = 173.3$ GeV as the top quark pole mass.

We have set the renormalization and factorization scales at $\sqrt{\hat{s}}$, the center-of-mass (CM) energy at the parton level, and adopted NN23LO Parton Distribution Functions (PDFs) [68,69]. including the $b$-flux, with $\alpha_s$ (the strong coupling constant with four-flavor schemes) evaluated consistently at all stages (i.e., convoluting PDFs, hard scattering, and decays). Parton shower (both initial and final), hadronization, heavy hadron decays, etc. have been dealt with by PYTHIA v.6.428 [70].

We consider all the light-flavor quarks, $b$-quarks, and gluons in the proton flux. The flavor-mixing, wherever
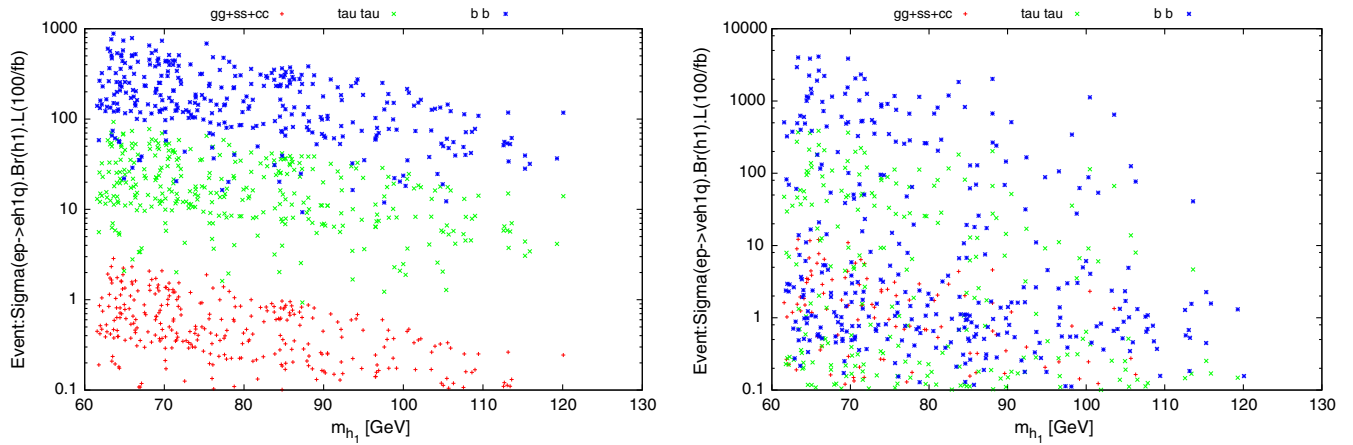


FIG. 5. Number of events in $e + 3$-jets (left panel) and $\not{E}_T + 3$-jets (right panel) channels at LHeC with integrated luminosity of 100 $fb^{-1}$.
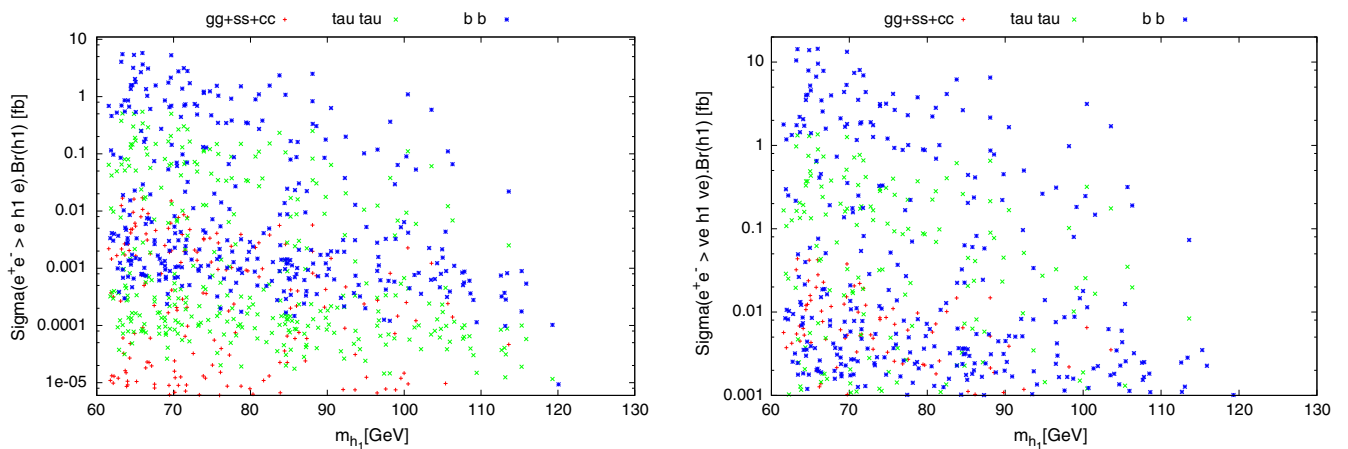


FIG. 6. The cross section multiplied with the Higgs branching ratios in units of $[fb]$ in the $e^+e^-$ LEP collider with center-of-mass energy 209 GeV, for the $\sigma(e^+e^- \to e^+ h_1 e^-)$ and $\sigma(e^+e^- \to \nu_e h_1 \bar{\nu}_e)$ in the left and right panels, respectively.
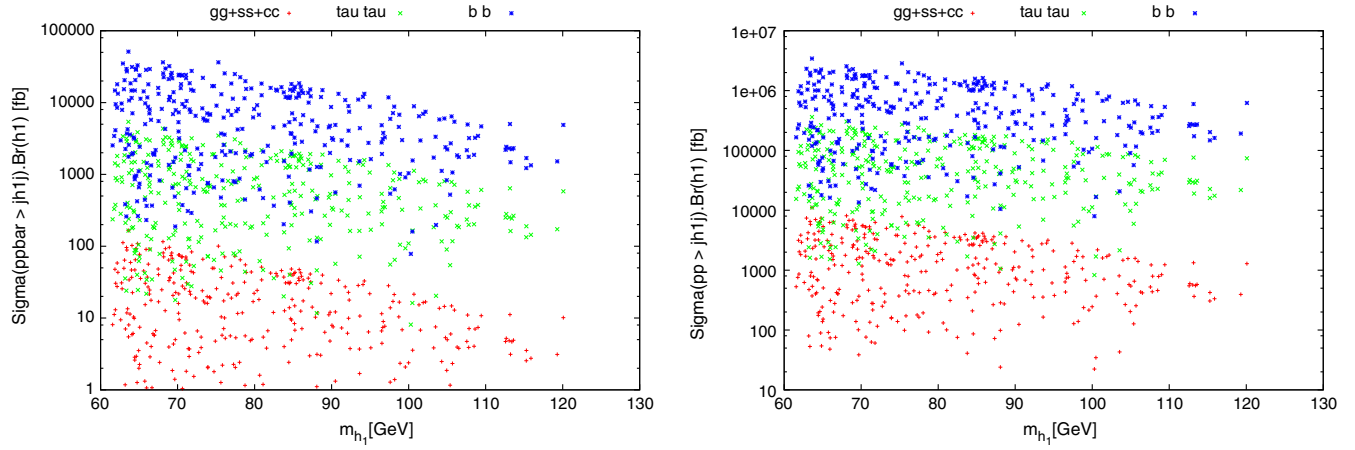
FIG. 7. Left panel: the cross section with Higgs branching ratios in units of [fb] at the Tevatron ($\sigma(p\bar{p} \to jh_1 j)$) with center-of-mass energy 1.96 TeV. Right panel: $\sigma(pp \to jh_1 j)$ at LHC collider with center-of-mass energy 14 TeV, where $j = $ u, d, c, s, b, g and their charge conjugation.

appropriate, is also considered for the allowed diagrams. Following this, it was realized that the signal processes have unique kinematic profiles, and we will discuss them below.

The cross section of the scattering $fa \to f'X$ via the gauge-boson ($V$) exchange can be expressed as

$$\sigma(fa \to f'X) \approx \int dx dp_T^2 P_{V/f}(x, p_T^2)\sigma(Va \to X), \quad (12)$$

where the fermion $f$ with a c.m. energy $E$ is radiating a gauge boson $V$ ($s \gg M_V^2$), $\sigma(Va \to X)$ is the cross section of the $Va \to X$ scattering, and $P_{V/f}$ can be viewed as the probability distribution for a weak boson $V$ of energy $xE$ and transverse momentum $p_T$. The dominant kinematical feature is a nearly collinear radiation of $V$ off $f$, termed as "Effective $W$-Approximation" [71]. The probability distributions of the weak bosons with different polarizations can be approximated by (in the limit of $s \gg M_V^2$)

$$P_{V/f}^T(x, p_T^2) = \frac{g_V^2 + g_A^2}{8\pi^2} \frac{1 + (1-x)^2}{x} \frac{p_T^2}{(p_T^2 + (1-x)M_V^2)^2},$$
$$(13)$$

$$P_{V/f}^L(x, p_T^2) = \frac{g_V^2 + g_A^2}{4\pi^2} \frac{1-x}{x} \frac{(1-x)M_V^2}{(p_T^2 + (1-x)M_V^2)^2}, \quad (14)$$

where $g_V(g_A)$ is the vector (axial) vector couplings of fermion-gauge-boson vertices.

From these equations, we can understand that the final state quark $f'$ typically has transverse momentum, $p_T \sim \sqrt{1-x}M_V \leq M_V$, i.e, less than the mass of the vector boson. Secondly, due to the $1/x$ behavior for the gauge-boson distribution, the outgoing parton energy $(1-x)E$ tends to be high and leads to a very high energetic forward jet, with a small angle (i.e., high forward rapidity) with

respect to the beam direction. Finally, at high $p_T$, the probabilities of the gauge bosons can be approximated as: $P_{V/f}^T \sim 1/p_T^2$ and $P_{V/f}^L \sim 1/p_T^4$. At high $p_T$ the longitudinally polarized gauge boson is relatively suppressed compared to the transversely polarized one. In particular, the first two criteria serve as guidance in our event selection for exploiting the kinematical features. Also, in both signals under consideration, the final state forward jet could be also a $b$-jet. However, as it is mostly in the forward region, with the tighter constraints of the rapidity of $b$-taggable jet, it hardly qualifies as $b$-tagged.

### B. Backgrounds

There are mainly two groups of SM backgrounds in our Higgs signals. The charged-current backgrounds consisting of $\nu t\bar{b}$, $\nu b\bar{b}j$, $\nu b2j$, $\nu 3j$, and the neutral-production ones identified as $e^- b\bar{b}j$, $e^- t\bar{t}$, $e^- bjj$, and $e^- jjj$. In all of these backgrounds the charge-conjugated processes are naturally implied.

For estimating the cross sections of these SM backgrounds, we used the same set of preselections, identical conventions, and parameter sets as for the signal. The expected number of the background events for 100 fb$^{-1}$ of integrated luminosity are given in the second column of Tables IV and VI.

### C. Signal-to-background analysis

We generated the SM backgrounds at the parton level using MADGRAPH V 2.4.3 [63] and then fed them to PYTHIA v.6.428 [70] for parton showering (both initial and final), hadronization, heavy hadron decays, etc. The initial state radiation (ISR) will reduce the total center-of-mass energy of the collision; however, at the LHeC with the main dynamics along the t-channel, the center-of-mass energy loss due to ISR has less impact. The top quark and $W$-boson

were allowed to decay freely within the PYTHIA program. The four-momentum of the jets is different as compared to the parton level quark due to the final state radiation (FSR), and in our analysis we considered the Gaussian type of smearing effects.

The LHeC detectors and their parameter considerations follow one of our recent analyses [38]. However,to be complete, let us describe it here briefly.

We have considered the experimental resolutions of the jet angles and energy using the toy calorimeter PYCELL, in accordance with the LHeC detector parameters, given in PYTHIA. As the invariant mass has been used to isolate the Higgs signal, this has some nontrivial effect. We considered LHC type of calorimeter for the LHeC. To be explicit, we set a somewhat symmetric detector coverage; however, in reality the electromagnetic and the hadronic calorimeters at LHeC, unlike ATLAS and CMS, are not exactly symmetric.

Since we are not doing detector simulation and also not considering the cracks in the detectors, we applied symmetric large rapidity coverage for jets and leptons.[5] We expect that these assumptions hardly alter our numerical findings. The detector parameters in PYCELL are set according to the LHeC detector [66]. Specifically, we assume large calorimeter coverage $|\eta| < 5.5$, with segmentation (the number of division in $\eta$ and $\phi$ are 320 and 200, respectively) $\Delta\eta \times \Delta\phi = 0.0359 \times 0.0314$. Furthermore, we have used Gaussian energy resolution [64] for electron and jets (labeled as $j$), with

$$\frac{\Delta E}{E} = \frac{a}{\sqrt{E}} \oplus b, \qquad (15)$$

where $a = 0.32$, $b = 0.086$ for jets, and $a = 0.085$, $b = 0.003$ for leptons, and $\oplus$ means addition in quadrature.

We have used a cone algorithm for the jet-finding, with jet radius $\Delta R(j) = \sqrt{\Delta\eta^2 + \Delta\phi^2} = 0.5$. Calorimeter cells with $E_{T,min}^{cell} \geq 5.0$ GeV are considered to be potential candidates for jet initiators. All cells with $E_{T,min}^{cell} \geq 1.0$ GeV were treated as part of the would-be jet. A jet is required to have minimum summed energy $E_{T,min}^j \geq 15$ GeV and the jets are ordered in $E_T$. The leptons ($\ell = e$ only) are selected if they satisfy the requirements: $E_T^\ell \geq 15$ GeV and $|\eta^\ell| \leq 3.0$. In our jet-finding algorithm, we include leptons as parts of jets. Finally, we separate them, putting some isolation criterion as follows: if we find a jet near a lepton, with $\Delta R(j - \ell) \leq 0.5$ and $0.8 \leq E_T^j/E_T^\ell \leq 1.2$, i.e. if the jet $E_T$ is nearly identical to that of this lepton, the jet is removed from the list of jets and treated as a lepton. However, if we find a jet within $\Delta R(j - \ell) \leq 0.5$ of a lepton, whose $E_T$ differs significantly from that of the lepton, the lepton is removed from the list

of leptons. This isolation criterion mostly removes leptons from $b$ or $c$ decays. We reconstructed the missing (transverse) energy ($\not{E}_T$) from all observed particles, and for the charge current the signal is shown in the right panel of Fig. 9. We have also calculated the same from the energy deposition in the calorimeter cells and found consistency between these two methods. Only jets with $|\eta^j| < 2.5$ and $E_T^j \geq 15$ GeV "matched" with a $b$-flavored hadron ($B$-hadron), i.e. with $\Delta R(j, B - \text{hadron}) < 0.2$ is considered to be "taggable". We assume that these jets are actually tagged with probability $\epsilon_b = 0.50$. We also adopted mistagging of non-$b$ jets as $b$-jets and treated $c$-jets differently from the gluon and light-flavor jets. A jet with $|\eta^j| \leq 2.5$ and $E_T^j \geq 15$ GeV matched with a $c$-flavored hadron ($C$-hadron, e.g., a $D$-meson or $\Lambda_c$-baryon), i.e., with $\Delta R(j, C - \text{hadron}) < 0.2$, is again considered to be taggable, with (mis)tagging probability $\epsilon_c = 0.10$. Jets that are associated with a $\tau$-lepton, with $\Delta R(j, \tau) \leq 0.2$, and all jets with $|\eta^j| > 2.5$, are taken to have vanishing tagging probability. All other jets with $E_T^j \geq 15$ GeV and $|\eta^j| \leq 2.5$ are assumed to be (mis)tagged with probability $\epsilon_{u,d,s,g} = 0.01$, following [36]. The overall analysis strategy has been adopted from [72–74].

### 1. e + 3-jet: electron channel

In this subsection we will analyze the neutral current signal electron channel, i.e., $e + 3$-jet, and apply different kinematical cuts to isolate the signal from the backgrounds.

(a) We first selected events containing at least three jets, i.e., $N_{jet} \gtrsim 3$, with $Pt_j > 15.0$ and $\eta_j < 5.5$. The distribution of the number of jets ($N_{jet}$) is shown in the left panel of Fig. 8. The efficiency of having $N_{jet} \gtrsim 3$, are approximately 40.0%, 42.8%, 45.3%, 45.6%, and 51.7%[6] for the signal benchmarks of $e1$ to $e5$, respectively. Since the two central jets originate directly from the Higgs boson itself, heavier masses lead to higher efficiencies. The jet selection criteria are the same for all the signals and corresponding backgrounds. Thus the jet efficiencies are identical in all backgrounds. Among all the backgrounds, $et\bar{t}$ leads to a total of six jets when both the top quarks decay hadronically—here the jet efficiency is maximal, about 92.2%. The next highest efficiency is from $\nu t b$, where the maximal number of jets is four. This leads to an efficiency around 60.7%. The jet efficiencies for the $ebbj$, $ebjj$, and $ejjj$ are between 7.0 to 10.0%, whereas for the $\nu bbj$, $\nu bjj$ and $\nu jjj$ channels, they range from 18.0 to 24.0%. In the neutrino cases, first of all there is no strict selection of neutrino momentum, unlike minimum transverse momentum requirements of the lepton, i.e., $e$ in this

---

[5]Here the lepton means only electron unless mentioned otherwise.

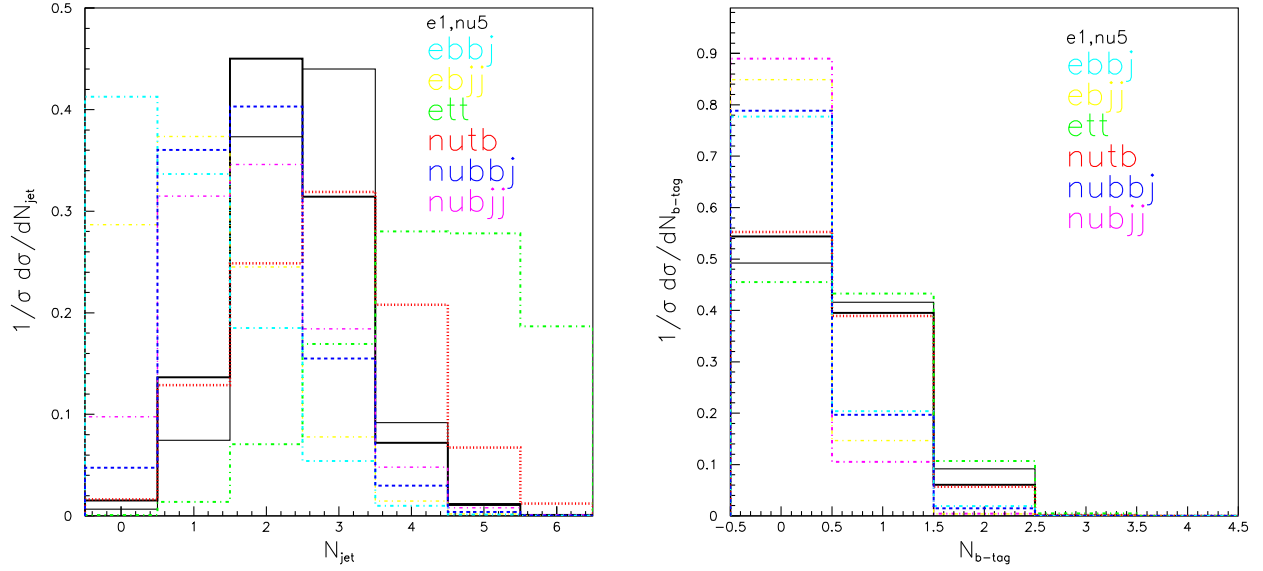[6]The efficiencies quoted here are with respect to the previous set of selections.

FIG. 8. Left panel: number of jet distributions for the $e1$ benchmark ($\nu5$ benchmark) in the $e + 3$-jets ($\not{E}_T + 3$-jets) channel using the thick (thin) black lines. Right panel: the number of $b$-tagged jet distribution is shown. Both of the distributions depend mainly upon the masses of the Higgs boson in two signal channels, i.e., the more massive the Higgs, the higher the number of jet peaks toward higher values. For all other signal benchmarks, the distributions follow a similar pattern and can be understood from the numerics in the corresponding columns in Tables IV and VI.

channel. Moreover the lepton-jet isolation criterion reduces the number of jets in the background with explicit lepton. This leads to the lower efficiency.

(b) We required one lepton ($e$) with $p_T > 15$ GeV and $\eta < 3.0$ as our signal is generated from the neutral current interaction. Since the lepton is originating from the $e$-beam, we required somewhat larger rapidity. The distribution of the number of leptons is shown in the left panel of Fig. 9. The lepton efficiency for all the signal benchmarks is approximately 94.0%, and for

the benchmarks where the Higgs mass is smaller, this lepton efficiency is larger as more collison energy is transferred to the lepton—however small it is, it does get reflected in the corresponding efficiencies. Among the backgrounds, the larger efficiency is for $e t\bar{t}$ with approximately 86.5%, as one top quark is allowed to decay leptonically whereas the other top quark must decay hadronically satisfying the three-jet criterion. The efficiencies for $ebbj$, $ebjj$, and $ejjj$ are between 76.9%–79.7%. The efficiency of $\nu tb$ is approximately
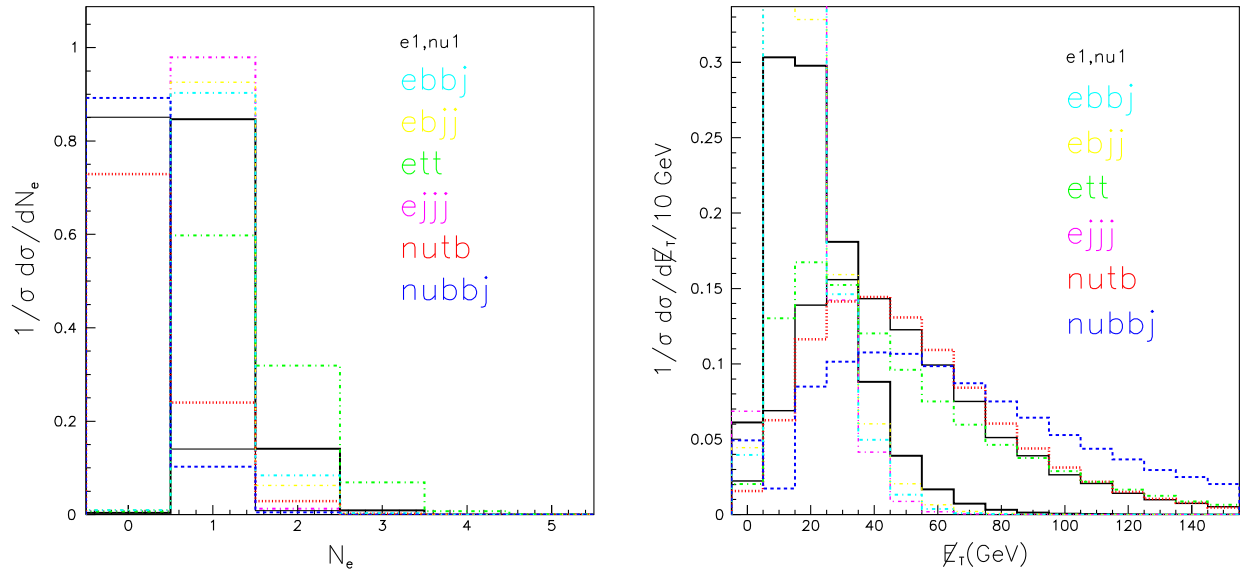


FIG. 9. Number of electron ($N_e$) distribution for the $e1$ benchmark ($\nu1$ benchmark) using thick (thin) black line in the left panel. The distribution of missing energy ($\not{E}_T$) for the $e1(\nu1)$ benchmark using thick (thin) black line in the right panel.

8.0%. This is close to the electron channel branching fraction, i.e., 10%. There are also secondary sources of electrons, like semileptonic $b$-decays or meson decays. Taking this into account, the transverse momentum and rapidity criterion reduces the efficiency to approximately 2%. The efficiency for $\nu bbj$ is approximately 2.8% where the source of the lepton is only from the semileptonic $b$-decay satisfying the isolation criterion or from secondary sources like meson or photon. The efficiency for $\nu bjj$ being 1.3% is just the half of $\nu bbj$ as it is clear from the presence of b-quark in these two cases. In case of $\nu jjj$, the lepton would only be coming from the secondary sources (meson or photon) during fragmentation and hadronization and the efficiency turns out to be approximately 0.002%.[7]

(c) We demanded at least two $b$-tagged jets with the inclusion of proper mistagging. The distributions of the number of $b$-tagged jets ($N_{b-tag}$) are shown in the right panel of Fig. 8. The efficiencies are approximately 13.7%, 13.8%, 14.4%, 14.1%, and 14.6% for the $e1$ to $e5$ benchmark points, respectively. In fact, all our signal benchmarks contain at least two $b$-quark. Since we considered $\epsilon_b = 0.50$, an approximately 10% lowering for the double $b$-tag is quite realistic due to the fact that not all $b$-quarks in the signal are eligible for the $b$-taggable criterion adopted in our analysis (another possibility is having a $c$-quark with $\epsilon_c = 0.10$ and a light flavored quark with $\epsilon_q = 0.01$).

Among the backgrounds, the irreducible one $ebbj$ has an efficiency of approximately 11.5%, roughly 2% less than the signal and this is mainly due to the rapidity acceptance of the taggable $b$-jet. Unlike the signal, the rapidity distribution of the two $b$-taggable jets for this background are not very central (i.e., we imposed the $\eta < 2.5$ a for taggable $b$-jets). For $etb$ and $\nu tb$, the efficiencies are approximately 11.6% and 10.0%, respectively whereas $\nu bbj$ and $\nu bjj$ have efficiencies of 8.2% and 2.4%. These $b$-tagged ratios with neutrinos follow very closely to the corresponding number efficiencies of $ebbj$ and $ebjj$. The efficiency of $ejjj$ is approximately 0.002 where low-flavor mistagging efficiencies with $\epsilon_c = 0.10$ and $\epsilon_q = 0.01$ ($q = u, d, s, g$) have been taken care of. We would expect similar $b$-tagged efficiencies (i.e, 0.002) for $\nu jjj$. However, as the lepton selection criteria (b) above severely reduced the number of events, the survived events hardly pass these $b$-tag criteria and $\nu jjj$ goes to zero level.

(d) In the central region, defined above in the selection (c), having the number of $b$-tagged jets greater than or equal to two (i.e., $N_b \lesssim 2$ with mistagging), we reconstruct all possible combinations of di-jet invariant masses, i.e., $M_{bb}$. Out of all possible combinations, we have chosen the best combinations for which the absolute difference, $|M_{bb} - M_{h_1}|$ is minimum. We identified these as the correct di-$b$-jet candidates for the Higgs boson. The distribution of $M_{bb}$ is shown in the left panel of Fig. 10 for the $e1$, $e3$, and $e5$ benchmark points. We have not shown explicitly the mass peaks of the $e2$ and $e4$ benchmark points, since they lie between the displayed peaks as the Higgs boson mass lies between the respective benchmarks (see Table III). The peaks of all the signal benchmarks always show up to the left side of the actual masses due to jet-energy smearing. Moreover, the shift depends on the jet-cone size under consideration: the larger the cone size the more the peak moves to the right. The price is having relatively less $N_{jet}$ efficiency in (a). The $M_{bb}$ distributions in Fig. 10 show a rapid fall on the higher side. Hence, we have selected events with some asymmetric mass windows: $M_{h_1} - 15.0\,\text{GeV} < M_{bb} < M_{h_1} + 5\,\text{GeV}$.[8]

For the signal, the efficiencies are approximately 54.0%, 47.7%, 43.3%, 38.7%, and 35.0% for the $e1$ to $e5$ benchmark points, respectively. The reconstructed Higgs boson mass tends to lie in the lower regions which depends mainly on the jet-cone size and the showering effects. Thus, the lower the benchmark Higgs boson mass, the larger the efficiency as can be seen from the second benchmark point.

The SM $ebbj$ processes have a $Z$-boson exchange resonant diagram with $Z \to b\bar{b}$. This leads to the appearances of the mass peaks around 60 GeV (approximately 30 GeV less than the $M_Z$ due to jet-energy smearing). The $\nu bjj$ mass peaks are somewhat similar to the $ebjj$, as this has a $W$ and/or $Z$-boson exchange resonant diagrams. As the Higgs boson mass is very close to the $W$-boson mass, at least in the $e1$ benchmark, the efficiencies are 32.5% and 25.4% for $\nu bjj$ and $ebjj$, respectively.

In the cases of $ett$ and $\nu tb$, the pure di-$b$-tagged jet is uncorrelated, and as a result the mass distributions are flat. However, it is not always the case that the primary hard $b$-jet or the secondary $b$-jet from the top quark decay are tagged. In the cases, of the hadronic top decay, i.e., W-hadronic decay, both can be mistagged and those combinations generally show

---

[7]Please note that we have not considered here the lepton mistagging efficiency from the jets. This is approximately 0.001% and having the three (or more) jets explicitly after considering the ISR and FSR, these efficiencies are somewhat consistent with the mistagging numbers with proper combinatorics.

[8]Please note that the $M_{bb}$ distributions are shown without imposing the mass window selection. The numbers start to differ from this column onwards as the Higgs mass window selection depends upon the Higgs boson masses of the corresponding benchmarks.
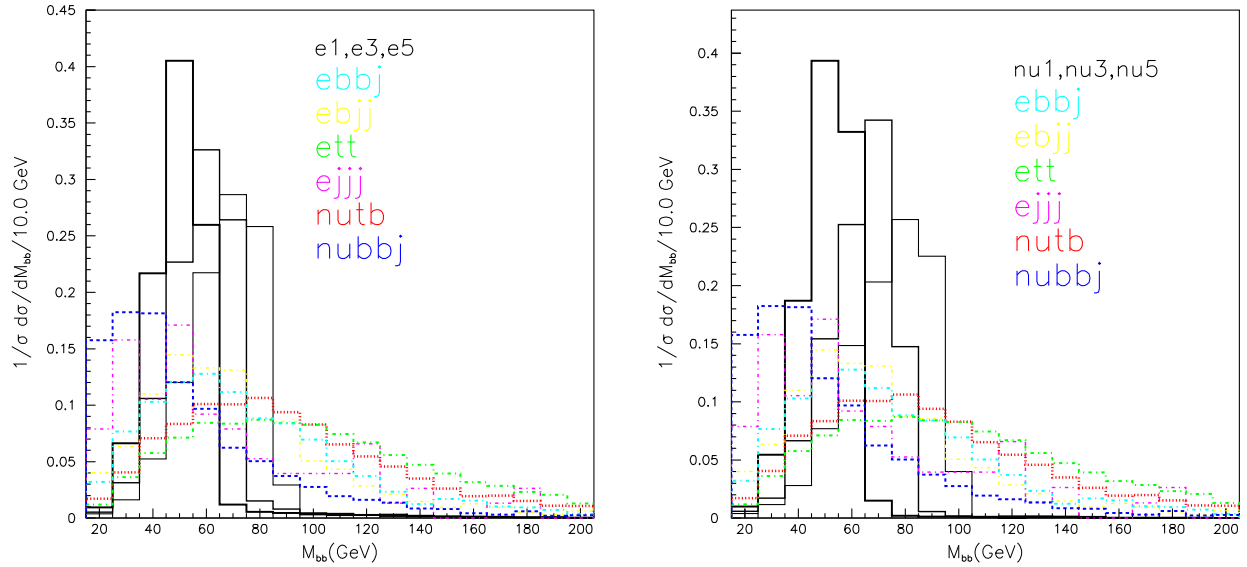
FIG. 10.    Left panel: the di-*b*-tagged invariant masses, $M_{bb}$, distribution for the $e + 3$-jets channel, for the $e1$, $e3$, and $e5$ benchmark points from left to right (thick to thinner), respectively. Right panel: similar to the $\not{E}_T + 3$-jets channel, with the mass peaks for $\nu1$, $\nu3$, and $\nu5$ from left to right (thick to thinner), respectively. See Table III for the corresponding Higgs boson masses.

the mass peaks around 80–90 GeV. The efficiencies of this selections are around approximately 15.3% and 18.1% for *ett* and *νtb*, respectively.

The efficiency for *ejjj* is approximately 18.2% and the mass distribution has a peak in the lower side. Due to this peak shift in the lower side, among all the benchmarks, the *ejjj* events survive better than those of the benchmarks with minimum Higgs boson mass.

(e)    We demanded that the remaining leading jet in the events should have $Pt_j > 15.0$ GeV with $-5.5 < \eta < -0.5$ [the values are chosen by inspecting the distribution shown in the left panel of Fig. 11 with a thick black line for the $e1$ benchmark and termed as the forward jet ($j_f$ or in the histogram as $jf$)]. The forward jet (the transverse momentum of the forward jet is shown in the left panel of Fig. 12) lies very close to the direction of the incoming proton; however, it also depends upon the Higgs mass for the given benchmarks. The more massive the Higgs boson is, the smaller the energy which remains for the forward jet as it lies close to the proton beam (larger rapidity). Vice versa, the less massive the Higgs, the larger the rapidity of the forward jet. With the exception of the $e2$ benchmark, the survival probability under this selection is larger with heavy Higgs boson masses. The backgrounds like *νtb* and *ett* generally have a large number of jets (shown in the left panel of Fig. 8). Thus, one out of many jets would likely pass this selection criterion, and, hence, the efficiencies are as large as the signal efficiency. The backgrounds *ebjj* and *νbjj* have somewhat similar efficiencies and are reduced maximally by this selection.

After applying this selection, the dominant remaining backgrounds are from the irreducible *ebbj*, *ebjj*, *νtb*, and a part from *ejjj* as the latter process has a big cross section to begin with.

(f)    We demand the magnitude of the product of the lepton and jet rapidity to be negative, i.e., $\eta_j.\eta_l < 0$. This is to say that they lie in the opposite hemispheres. For this selection, the efficiencies for the $e1$ to $e5$ signal benchmarks vary, as 53.9%, 55.2%, 55.9%, 57.8%, and 55.8%, respectively. This selection reduces the high multiplicity backgrounds severely. For example, *νtb* (*ett*) survived by approximately 1.5% (39.5%).

(g)    Like the forward jet cut mentioned above in item (e), we assume the rapidity of the lepton to be in the forward region since the lepton in the signal source is directly from the *e*-beam.[9] The transverse momentum of the forward lepton is shown in the right panel of Fig. 12. By inspecting the rapidity distribution of this lepton shown in the right panel of Fig. 11, we selected events with lepton rapidity within the range $-2.5 < \eta < 2.0$. The lepton satisfying this criterion is called the forward lepton ($e_f$). The signal events which survived this criterion are approximately 94.0% while for *νtb* it reduces to approximately 70%–85% as the source of the lepton in this case is the top quark decay and there is no guarantee that the lepton should be in

---

[9]Please note that the lepton (i.e, *e*) and the forward jet ($j_f$) are likely to be in the opposite hemispheres; i.e., if the jet is in the forward region then the lepton will be in the backward region or vice versa. This is also reflected in the rapidity distributions in the left and right panels of Fig. 11.

TABLE III.    The selected NMSSM benchmark points obtained using MNSSMTOOLS 5.0.1 [49] to find the $h_1$ signal at LHeC. The values displayed are at the electroweak scale. The following parameters are fixed: $M_3 = 1800$ GeV, $A_\tau = A_\ell = 1500$ GeV and $M_{\tilde{e}} = 300$ GeV. Please note that we used $M_A$ and $M_P$ as inputs—thus our scenario is not the $Z_3$-NMSSM, and for that, $\xi_F$ and $\xi_S$ are nonzero and also given in the table. We mention the cross section $\sigma \times \mathrm{BR}(h_1 \to b\bar{b})$ (as $\sigma.BR$) at LHeC. Please note that the $e5$ benchmark for $e + 3$-jets and the $\nu4$ benchmark for $\not{E}_T + 3$-jets is identical.

| Benchmark points | e1 | e2 | e3 | e4 | e5 | ν1 | ν2 | ν3 | ν4 = e5 | ν5 |
|---|---|---|---|---|---|---|---|---|---|---|
| $\lambda$ | 0.241 | 0.168 | 0.171 | 0.237 | 0.384 | 0.208 | 0.263 | 0.296 | 0.384 | 0.498 |
| $\kappa$ | 0.371 | 0.0567 | 0.0324 | 0.0384 | 0.0152 | 0.0577 | 0.143 | 0.147 | 0.0152 | 0.291 |
| $\tan\beta$ | 56.71 | 48.62 | 56.32 | 56.27 | 4.41 | 3.81 | 4.95 | 5.15 | 4.41 | 6.18 |
| $A_\lambda$ (GeV) | 974.0 | 1007.8 | 1230.8 | 964.1 | 1222.4 | 1130.3 | 1105.8 | 1078.3 | 1222.4 | 1107.8 |
| $A_\kappa$ (GeV) | −1139.2 | −1105.6 | −1214.2 | −1108.3 | −1062.3 | −1230.3 | −835.9 | −803.6 | −1062.3 | −1732.7 |
| $\mu_{\mathrm{eff}}$ | 466.4 | 272.9 | 297.2 | 454.6 | 381.1 | 392.6 | 374.5 | 342.7 | 381.1 | 193.8 |
| $M_1$ (GeV) | 274.6 | 347.5 | 241.7 | 272.5 | 335.3 | 173.3 | 146.5 | 172.7 | 335.3 | 112.1 |
| $M_2$ (GeV) | 293.4 | 482.3 | 462.5 | 277.5 | 352.3 | 283.9 | 257.3 | 495.3 | 352.3 | 430.7 |
| $M_{\tilde{q}}$ | 1010.4 | 941.9 | 700.6 | 1036.6 | 734.0 | 807.1 | 812.9 | 772.5 | 734.0 | 762.0 |
| $A_t = A_b$ (GeV) | −2661.8 | −1695.4 | −1735.6 | −2679.4 | −1585.1 | −1946.3 | −1883.7 | −1676.3 | −1585.1 | −1894.7 |
| $M_A$ (GeV) | 316.9 | 282.2 | 239.8 | 319.9 | 125.6 | 102.9 | 106.9 | 131.7 | 125.6 | 134.5 |
| $M_P$ (GeV) | 2015.5 | 1650.2 | 1995.9 | 2019.2 | 2396.3 | 1660.2 | 2429.6 | 1474.9 | 2396.3 | 1858.8 |
| $\xi_F$ ($10^6$ GeV$^2$) | −2.01 | −1.77 | −2.23 | −1.98 | −1.21 | −2.32 | −1.85 | −1.43 | −1.21 | −0.47 |
| $\xi_S$ ($10^9$ GeV$^3$) | −6.79 | −3.27 | −6.06 | −6.77 | −5.56 | −3.42 | −6.15 | −1.06 | −5.56 | −0.89 |
| $m_{\tilde{\chi}_1^0}$ (GeV) | 142.2 | 181.9 | 112.1 | 146.3 | 33.7 | 164.5 | 139.5 | 163.6 | 33.7 | 94.2 |
| $m_{h_1}$ (GeV) | 63.59 | 70.59 | 75.29 | 82.24 | 88.07 | 65.93 | 71.32 | 83.77 | 88.07 | 100.47 |
| $m_{h_2}$ (GeV) | 122.9 | 122.7 | 122.8 | 123.6 | 126.1 | 127.8 | 126.5 | 124.6 | 126.1 | 125.4 |
| $m_{h_3}$ (GeV) | 1858.7 | 1394.5 | 1852.1 | 1861.1 | 2365.0 | 1315.5 | 2078.4 | 950.1 | 2365.0 | 1467.3 |
| $m_{a_1}$ (GeV) | 67.8 | 73.4 | 77.8 | 85.3 | 89.0 | 73.9 | 78.2 | 107.1 | 89.0 | 118.9 |
| $m_{a_2}$ (GeV) | 2014.3 | 1649.4 | 1995.2 | 2018.0 | 2393.3 | 1659.6 | 2427.6 | 1473.5 | 2393.3 | 1848.9 |
| $m_{h^\pm}$ (GeV) | 112.4 | 114.9 | 121.6 | 124.1 | 103.3 | 102.9 | 101.4 | 124.8 | 103.3 | 120.1 |
| $\mathrm{BR}(h_1 \to b\bar{b})$ | 0.902 | 0.910 | 0.909 | 0.901 | 0.828 | 0.910 | 0.909 | 0.906 | 0.828 | 0.907 |
| $\sigma$ [fb] | 9.783 | 5.627 | 7.535 | 4.815 | 4.628 | 45.209 | 25.561 | 20.205 | 24.371 | 12.403 |
| $\sigma.BR$[fb] | 8.824 | 5.121 | 6.850 | 4.338 | 3.832 | 41.141 | 23.235 | 18.306 | 20.180 | 11.250 |

the forward direction with the imposed criterion. The background $ett$ would be maximally three leptons, and it is likely that one out of three leptons will pass the forward rapidity criterion $-2.5 < \eta < 2.0$. Thus, one would expect large survival probability which is indeed approximately 80%. In Table IV, we tabulated the events after imposing the rapidity gap between the forward lepton and forward jet, i.e., $\Delta\eta_{jf-ef}$. We have shown the distribution of rapidity of the lepton in the right panel of Fig. 11 and the rapidity differences with the jet in the left panel of Fig. 13. We demanded $-5.5 < \Delta\eta_{jf-ef} < 0.5$, and due to that the signal benchmarks reduced by approximately 2.0–3.0%. All the SM backgrounds remain the same except the $ebjj$ changes from 93.3%, 94.9%, 95.7%, 99.2%, and 96.1% for the $e1$ to $e5$ signal benchmarks, respectively.

(h) For the di-$b$-jet, for which $M_{h_1} = m_{bb}$ as in the selection (d) above and with the forward tagged jet ($j_f$), we reconstructed three-jet invariant mass, $m_{h_1 j_f} = m_{bb j_f}$. This essentially reflects the overall

energy scale of the hard scattering. The distributions are shown in the right panel of Fig. 13. We impose the condition $m_{h_1 j_f} > 190$ GeV. With this selection the signal events for all the benchmarks remain approximately 50.2–54.5%. The most dominant irreducible background $ebbj$ remains approximately 14.0%–24.0%, whereas $ebjj$ remains approximately 7.0% or less. The backgrounds $ett$ remains approximately 8.0% or less. The $\nu t b$ becomes zero.

At this stage the most dominant backgrounds which remain are: $ebbj$, $ebjj$ (at the level of signal events), and $ejjj$.

(i) We devised another set for selection based on the sum of the transverse momentum of all jets present in the events, $H_T = \sum |Pt_j|$. The distribution is shown in the left panel of Fig. 14. The signal shows the peak around 100 GeV. The $\nu t b$ shows a peak around 125 GeV whereas $ett$ displays it around 250 GeV; the higher value reflects the presence of a higher number of jets. We demanded a selection of $H_T > 100$ GeV. The number of signal events for all the benchmarks remains
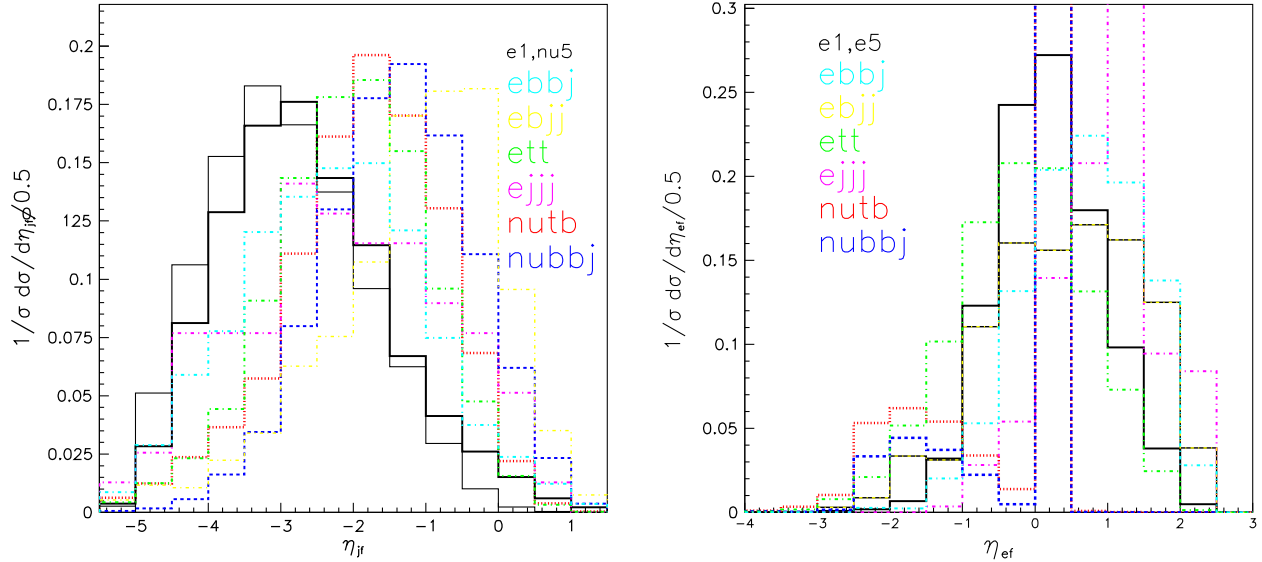
FIG. 11.  Left panel: the rapidity of the forward jet ($\eta_{jf}$) for the $e1$ and $\nu5$ signal benchmark points. The distributions for other benchmarks lie between these distribution profiles. Right panel: the rapidity of the forward lepton ($\eta_{ef}$) for the $e1$ and $e5$ benchmark points (somewhat similar for other benchmarks).

approximately 95.0%–98.0% (for heavy Higgs boson masses the survival event probabilities are more). We see that this selection is not reducing much of *ett*, at most 2.0%. However this background is not big at this stage. The *ebjj* contribution is also not much; it survived by, at most, 75.0% for the *e5* benchmark. With this selection, *ebbj* is reduced to approximately 52.2%, 55.6%, 64.0%, 65.5%, and 73.9% for the *e1* to *e5* benchmark points, respectively. In spite of a large reduction, *ebbj* is the only dominant contribution at this stage.

(j) Finally, to suppress the *ebbj* further, we devise a new kinematical variable by adding the vector component of three-momentum of all the jets present in the event. This is defined as: $\vec{H}_T = \sum \vec{P}t_j$. The distribution is shown in the right panel of Fig. 14, and it is evident that here the peaks are at a lower value of $|\vec{H}_T|$, as compared to the left panel of the same figure ($H_T$ is defined in selection (i) above). In the events having more jets, the jets are naturally distributed symmetrically in the $\eta - \phi$ plane. These regular



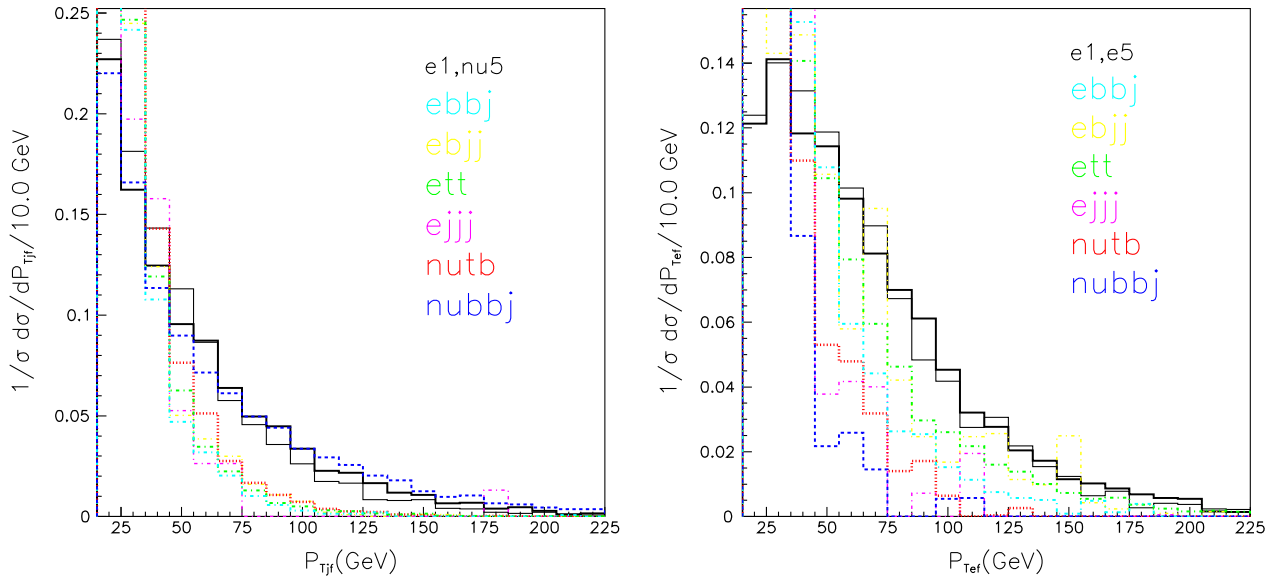FIG. 12.  Left panel: the transverse momentum ($P_T$) of forward jet ($P_{Tjf}$) for the $e1$ and $\nu5$ signal benchmarks. Right panel: the same for the forward lepton ($P_{Tef}$) only in the electron channel for the $e1$ and $e5$ signal benchmarks.

TABLE IV.   The number of signal and background events $e + 3$-jet channel after a cumulative set of selections at the LHeC collider with 100 fb$^{-1}$ integrated luminosity for selective benchmark points consistent with all the phenomenological, sparticle masses, relic density of cold-dark matter, direct and indirect dark matter searches, and the most up-to-date Higgs boson data. We simulated each benchmark signal with 200K and each background with 400K Monte Carlo simulated events. In the second column "RawEvt" stands for the number of events with only the generator-level cuts (Eq. (11) imposed for the signal as well as for backgrounds. For signal benchmarks, the proper branching factor, $h_1 \to b\bar{b}$ has been multiplied with the total cross section and for backgrounds with $W$-boson and $t$-quark we assume a free decay. In the final column we list the significance ($\mathcal{S}$) defined as $\mathcal{S} = S/\sqrt{B}$, where $S(B)$ stands for signal (background) events for 100 fb$^{-1}$ of data after all cuts mentioned in the "j" column are implemented. The significances for 1000 fb$^{-1}$ are shown in the parentheses.

| Proc, $m_h$ | RawEvt | a | b | c | d | e | f | g | h | i | j | $\mathcal{S}$ |
|---|---|---|---|---|---|---|---|---|---|---|---|---|
| e1,63.59 | 882.4 | 351.2 | 330.0 | 45.3 | 24.5 | 23.9 | 12.8 | 12.5 | 6.3 | 6.0 | 2.2 | 0.40(1.3) |
| ebbj | 268 839 0.0 | 176 102.0 | 135 388.5 | 155 30.5 | 3759.5 | 3461.2 | 2655.6 | 2476.5 | 343.1 | 179.0 | 29.8 | B=30.8 |
| ebjj | 330 834.0 | 31317.5 | 233 81.6 | 575.6 | 146.4 | 110.8 | 74.4 | 73.6 | 3.3 | 2.5 | 0.8 | |
| et$\bar{t}$ | 1425.5 | 1313.8 | 1136.9 | 131.8 | 20.2 | 19.9 | 7.9 | 7.8 | 0.4 | 0.4 | 0.2 | |
| ejjj | 372 241 00.0 | 494 304 9.0 | 394 009 7.5 | 8862.8 | 1611.4 | 966.9 | 805.7 | 805.7 | 161.1 | 0.0 | 0.0 | |
| νbbj | 213 85.4 | 4040.5 | 112.0 | 10.9 | 2.2 | 1.8 | 0.0 | 0.0 | 0.0 | 0.0 | 0.0 | |
| νbjj | 4077.8 | 985.1 | 13.3 | 0.4 | 0.1 | 0.1 | 0.0 | 0.0 | 0.0 | 0.0 | 0.0 | |
| νtb | 843 95.2 | 512 27.5 | 3848.3 | 405.4 | 73.3 | 70.6 | 0.7 | 0.7 | 0.0 | 0.0 | 0.0 | |
| νjjj | 387 092 0.0 | 718 974.7 | 1675.5 | 0.0 | 0.0 | 0.0 | 0.0 | 0.0 | 0.0 | 0.0 | 0.0 | |
| e2, 70.59 | 512.1 | 219.2 | 206.2 | 28.4 | 13.6 | 13.2 | 7.3 | 7.2 | 3.8 | 3.6 | 1.3 | 0.33(1.0) |
| ebbj | 268 839 0.0 | 176 102.0 | 135 388.5 | 155 30.5 | 3505.9 | 3222.5 | 2357.2 | 2222.9 | 402.8 | 223.8 | 14.9 | B=16.0 |
| ebjj | 330 834.0 | 313 17.5 | 233 81.6 | 575.6 | 142.3 | 100.9 | 64.5 | 64.5 | 3.3 | 0.8 | 0.8 | |
| et$\bar{t}$ | 1425.5 | 1313.8 | 1136.9 | 131.8 | 20.9 | 20.7 | 8.2 | 8.1 | 0.5 | 0.5 | 0.3 | |
| ejjj | 372 241 00.0 | 494 3049.0 | 394 009 7.5 | 8862.8 | 1611.4 | 1128.0 | 1128.0 | 1128.0 | 161.1 | 0.0 | 0.0 | |
| νbbj | 213 85.4 | 4040.5 | 112.0 | 10.9 | 1.7 | 1.3 | 0.0 | 0.0 | 0.0 | 0.0 | 0.0 | |
| νbjj | 4077.8 | 985.1 | 13.3 | 0.4 | 0.1 | 0.1 | 0.0 | 0.0 | 0.0 | 0.0 | 0.0 | |
| νtb | 843 95.2 | 512 27.5 | 3848.3 | 405.4 | 74.7 | 71.9 | 2.1 | 2.1 | 0.0 | 0.0 | 0.0 | |
| νjjj | 387 092 0.0 | 718 974.7 | 1675.5 | 0.0 | 0.0 | 0.0 | 0.0 | 0.0 | 0.0 | 0.0 | 0.0 | |
| e3, 75.29 | 685.0 | 310.1 | 291.6 | 42.0 | 18.2 | 17.9 | 10.0 | 9.8 | 4.9 | 4.7 | 1.5 | 0.38(1.2) |
| ebbj | 268 839 0.0 | 176 102.0 | 135 388.5 | 155 30.5 | 3147.9 | 2894.3 | 2103.6 | 1999.1 | 373.0 | 238.7 | 14.9 | B=16.0 |
| ebjj | 330 834.0 | 313 17.5 | 233 81.6 | 575.6 | 134.0 | 97.6 | 63.7 | 63.7 | 2.5 | 0.8 | 0.8 | |
| et$\bar{t}$ | 142 5.5 | 131 3.8 | 113 6.9 | 131.8 | 21.4 | 21.1 | 8.4 | 8.3 | 0.6 | 0.5 | 0.3 | |
| ejjj | 372 241 00.0 | 494 304 9.0 | 394 009 7.5 | 8862.8 | 1611.4 | 1128.0 | 966.9 | 966.9 | 161.1 | 0.0 | 0.0 | |
| νbbj | 213 85.4 | 4040.5 | 112.0 | 10.9 | 1.4 | 1.0 | 0.0 | 0.0 | 0.0 | 0.0 | 0.0 | |
| νbjj | 4077.8 | 985.1 | 13.3 | 0.4 | 0.1 | 0.1 | 0.0 | 0.0 | 0.0 | 0.0 | 0.0 | |
| νtb | 843 95.2 | 512 27.5 | 3848.3 | 405.4 | 78.2 | 75.4 | 2.1 | 2.1 | 0.0 | 0.0 | 0.0 | |
| νjjj | 387 092 0.0 | 718 974.7 | 1675.5 | 0.0 | 0.0 | 0.0 | 0.0 | 0.0 | 0.0 | 0.0 | 0.0 | |
| e4, 82.24 | 433.8 | 210.9 | 198.6 | 28.0 | 10.8 | 10.6 | 6.2 | 6.0 | 3.3 | 3.1 | 1.1 | 0.28(0.9) |
| ebbj | 268 839 0.0 | 176 102.0 | 135 388.5 | 155 30.5 | 2745.1 | 2566.0 | 1879.8 | 1849.9 | 432.6 | 283.5 | 14.9 | B=15.3 |
| ebjj | 330 834.0 | 313 17.5 | 233 81.6 | 575.6 | 130.7 | 93.5 | 60.4 | 60.4 | 1.7 | 0.0 | 0.0 | |
| et$\bar{t}$ | 1425.5 | 1313.8 | 1136.9 | 131.8 | 21.3 | 21.1 | 8.3 | 8.2 | 0.6 | 0.6 | 0.4 | |
| ejjj | 372 241 00.0 | 494 304 9.0 | 394 009 7.5 | 8862.8 | 1450.3 | 1128.0 | 966.9 | 966.9 | 322.3 | 161.1 | 0.0 | |
| νbbj | 213 85.4 | 4040.5 | 112.0 | 10.9 | 1.2 | 0.7 | 0.0 | 0.0 | 0.0 | 0.0 | 0.0 | |
| νbjj | 4077.8 | 985.1 | 13.3 | 0.4 | 0.1 | 0.1 | 0.0 | 0.0 | 0.0 | 0.0 | 0.0 | |
| νtb | 843 95.2 | 512 27.5 | 3848.3 | 405.4 | 78.9 | 78.2 | 2.1 | 2.1 | 0.0 | 0.0 | 0.0 | |
| νjjj | 387 092 0.0 | 718 974.7 | 1675.5 | 0.0 | 0.0 | 0.0 | 0.0 | 0.0 | 0.0 | 0.0 | 0.0 | |
| e5, 88.07 | 383.2 | 198.0 | 186.2 | 27.2 | 9.5 | 9.3 | 5.2 | 6.1 | 2.6 | 2.6 | 0.83 | 0.12(0.4) |
| ebbj | 268 839 0.0 | 176 102.0 | 135 388.5 | 155 30.5 | 2700.3 | 2506.4 | 1894.7 | 1820.1 | 343.1 | 253.6 | 44.8 | B=45.2 |
| ebjj | 330 834.0 | 313 17.5 | 233 81.6 | 575.6 | 112.5 | 80.2 | 49.6 | 48.8 | 3.3 | 2.5 | 0.0 | |
| et$\bar{t}$ | 1425.5 | 1313.8 | 1136.9 | 131.8 | 21.4 | 21.2 | 8.3 | 8.2 | 0.7 | 0.7 | 0.4 | |
| ejjj | 372 241 00.0 | 494 304 9.0 | 394 009 7.5 | 8862.8 | 966.9 | 966.9 | 805.7 | 805.7 | 322.3 | 161.1 | 0.0 | |
| νbbj | 213 85.4 | 4040.5 | 112.0 | 10.9 | 1.1 | 0.8 | 0.0 | 0.0 | 0.0 | 0.0 | 0.0 | |
| νbjj | 4077.8 | 985.1 | 13.3 | 0.4 | 0.1 | 0.1 | 0.0 | 0.0 | 0.0 | 0.0 | 0.0 | |
| νtb | 843 95.2 | 512 27.5 | 3848.3 | 405.4 | 86.5 | 85.8 | 1.4 | 1.4 | 0.0 | 0.0 | 0.0 | |
| νjjj | 387 092 0.0 | 718 974.7 | 1675.5 | 0.0 | 0.0 | 0.0 | 0.0 | 0.0 | 0.0 | 0.0 | 0.0 | |
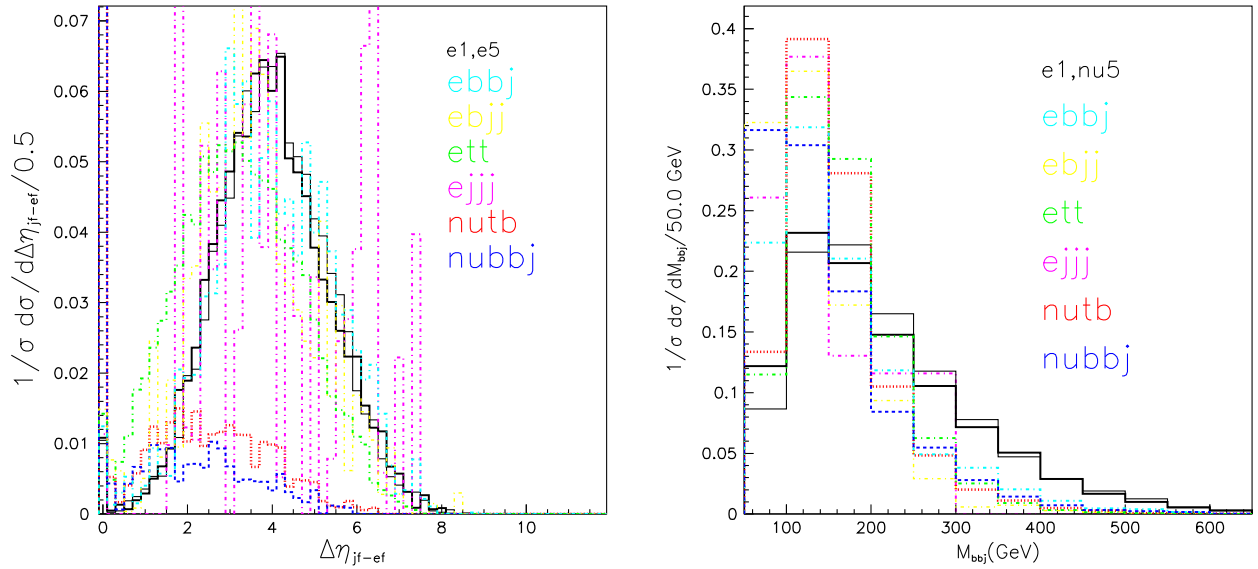
FIG. 13. Left panel: the rapidity differences between forward jet ($j_f = jf$) and forward lepton ($e_f = ef$), i.e., $\Delta\eta_{jf-ef}$ only for the $e1$ and $e5$ signal benchmarks in the electron channel. The signal shows a large rapidity gap. Right panel: The invariant masses of the Higgs candidate jets, $M_{bb}$ shown in Fig. 10, together with the forward jet, i.e., $M_{bbj_f} = m_{h_1 j_f}$ for both the signal channels for the $e1$ benchmark ($\nu5$ benchmark) using thick(thin) black lines. The signal distributions in both channels do not differ as the electron and $\not{E}_T$ do not have a direct big role in reconstructing the three-jet invariant mass. The distributions for other signal benchmarks in both of the channels are somewhat identical.

arrangements of jets three-momentum tend to cancel each other out, which leads to a lower magnitude of $\vec{H}_T$. For example, for *ett*, $\nu tb$ the peaks are around 40 GeV, while for the *ebbj*, *ebjj*, and *ejjj*, they are around 25 GeV or less. By demanding the magnitude of $|\vec{H}_T| > 50$ GeV, the signals are reduced by approximately 30.0%–35.0%. The background *ebbj* is reduced severely by approximately 85%–95%.
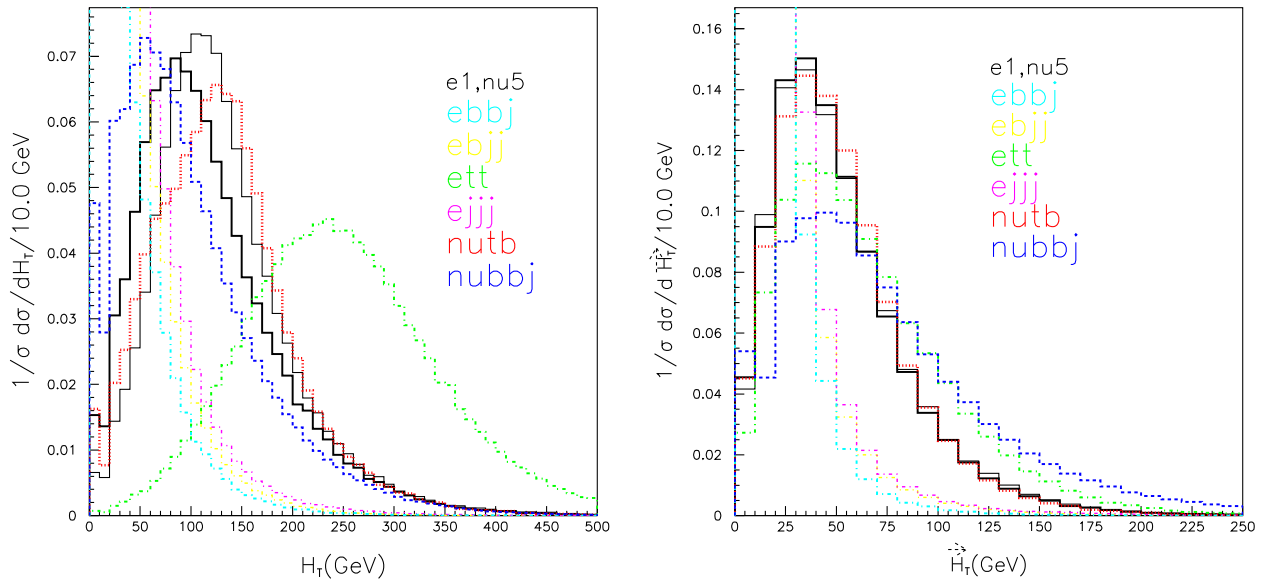


FIG. 14. Left panel: $H_T = \sum |Pt_j|$ distribution for the $e1$ benchmark and the $\nu5$ benchmark. The distributions for other signal benchmarks in both of the channels are somewhat identical. Right panel: $\vec{H}_T = |\sum \vec{P}t_j|$ defined (in the figure, the magnitude of the vector is naturally implied) in kinematical selection (i), for the leptonic and missing energy channels (the presence of the lepton or $\not{E}_T$ do not matter directly for the $\vec{H}_T$ distribution; however, the number of jets does.) for the $e1$ and $\nu5$ benchmark points. The distributions for other benchmarks in both of the signal channels are somewhat similar.

TABLE V. The optimization of the signal channel with different sets of kinematical selection cuts, e.g., $\eta_l$, $\Delta\eta_{jl}$, $m_{\phi j}$, $H_T$, magnitude of vector $\overrightarrow{H_T}$ (see text for details) with the best significance obtained for 100 fb$^{-1}$. In the right-hand columns, we strictly required that the number of signal events must be greater than ten or at least approximately five for the low luminosity options. The significances in the parentheses are for 1000 fb$^{-1}$.

| BP, $m_h$ | $\eta_l, \Delta\eta_{jl}, m_{\phi j}, H_T, \vec{H}_T$ | S | B | $\mathcal{S}$ | $\eta_l, \Delta\eta_{jl}, m_{\phi j}, H_T, \vec{H}_T$ | S | B | $\mathcal{S}$ |
|---|---|---|---|---|---|---|---|---|
| $e1, 63.59$ | $(1.0,-1.0),(0.0,-4.3),180,130,60$ | 4.9 | 162.3 | 0.38(1.2) | $(1.6,-2.5),(0.3,-6.0),100,140,30$ | 12.8 | 412.7 | 0.63(1.99) |
| $e2, 70.59$ | $(1.0,-1.0),(0.0,-3.0),180,140,60$ | 2.7 | 1.3 | 2.36(7.5) | $(1.1,-2.5),(0.2,-5.7),90,90,30$ | 10.1 | 1295.3 | 0.28(0.89) |
| $e3, 75.29$ | $(1.0,-2.5),(0.4,-3.4),180,140,60$ | 3.1 | 1.5 | 2.53(8.0) | $(1.0,-2.1),(0.4,-6.0),120,110,30$ | 11.6 | 565.2 | 0.49(1.54) |
| $e4, 82.24$ | $(1.0,-1.4),(0.0,-3.4),180,140,60$ | 1.6 | 0.6 | 2.09(6.6) | $(1.0,-2.1),(0.1,-3.4),110,140,30$ | 4.1 | 154.1 | 0.32(1.00) |
| $e5, 88.07$ | $(1.0,-1.8),(0.0,-3.0),180,140,60$ | 1.3 | 2.4 | 0.85(2.7) | $(1.3,-2.1),(0.1,-5.9),150,140,30$ | 4.8 | 340.0 | 0.26(0.82) |

After applying the cumulative selection from (a)–(j), we estimated the total SM background events to be found in the final column of Table IV. The significance for the 100 $fb^{-1}$ integrated luminosity is approximately $0.40 - 0.12\sigma$. This is not good enough to ensure the finding of a Higgs boson. However, at the end of LHeC data accumulation with approximately 1000 $fb^{-1}$, the significances (quoted in the parentheses) improve to become $1.3 - 0.4\sigma$. Notice that the significances do not scale accordingly with the Higgs masses. For example, the mass of the Higgs boson in the $e2$ benchmark is less than the $e3$ benchmark, thus one would expect the larger cross section in the $e2$ benchmark. This is mainly because of the parameter spaces dependent couplings of the $ZZh_1$ in the gauge-boson fusion type of production. For the $e2$ benchmark, the values of $ZZh_1$ coupling are less with respect to the $e3$ benchmark.

It is somewhat clear from Table IV that the significances in the electron channel are not very promising for the cut-based cumulative selections. To find better significances, we exploited some kind of optimization technique. First of all, we selected the following kinematical variables: $\eta_l$ (rapidity of the forward lepton); $\Delta\eta_{jl} = \eta_{j_f} - \eta_{l_f}$ (the rapidity differences between the forward jet and forward lepton); $m_{\phi j}$ (three jet invariant masses, i.e., two Higgs boson candidate jets and one forward jet); $H_T$ (the scalar sum of the transverse momentum of the jets); $|\vec{H}_T|$ (the vector sum of the transverse momentum of the jets). The optimization starts with the events which passed the forward jet criteria (after selection criterion e). The numerical values of all these kinematical variables are varied within a maximum and minimum range (by seeing the corresponding distributions). In particular, we varied the following kinematical ranges: upper values of $\eta_l$ in the range $(1.0,2.5)$ with step size 0.1 and the lower values in $(-2.5,-1.0)$ with step size 0.1; the upper values of $\Delta\eta_{jl}$ in $(0.0,1.5)$ with step size 0.1, while the lower values in $(-6.0,-3.0)$ with step size 0.1; $m_{\phi j}$ in $(80.0,180.0)$ with step size 10.0; $H_T$ in $(70.0,140.0)$ with step size 10.0; and $|\vec{H}_T|$ in $(30.0,60.0)$ with step size 10.0. We have

checked approximately 44695552 combinations and estimated the numbers of signal events and the total SM backgrounds and, finally, the significances.

The kinematical selection configurations and their numerical values for which the significances (in the fifth and ninth columns) for integrated luminosity of 100 fb$^{-1}$ are maximum is shown in Table V. It turns out that for Higgs boson masses up to 82.0 GeV, the significances reach at approximately $2.1\sigma$. In the right panel, we demanded that the number of signal events be at least ten for the low luminosity option (for Higgs masses greater than 80.0 GeV, we found approximately five signal events) and for that the number of backgrounds is also large. It is clear that for the Higgs boson masses of approximately 65.0 GeV, the significances could be 0.60 (2.0)$\sigma$ for 100(1000) fb$^{-1}$.

As the neutral current signal, discussed above, does not have large significances in simple cut-based selection, we turn our attention to the charged current mode. It is clear from the right panel of Fig. 5 that the event rates are high enough to consider this case.

### 2. $\not{E}_T$ + 3-jet: missing-energy channel

We are now looking for the feasibility of finding the Higgs boson in the $\not{E}_T$ + 3-jet. Like in the $e$ + 3-jet discussed in the previous sections, we apply kinematical cuts to isolate the beyond SM-type Higgs boson signal from the backgrounds. These cuts are, however, slightly different. The number of signal and SM background events is tabulated in Table VI.

(A) We first selected events containing at least three jets, i.e., $N_{jet} \gtrsim 3$. The distribution of the number of jets ($N_{jet}$) is shown (only for the $\nu 5$ benchmark) in the left panel of Fig. 8. The jet reconstruction criteria are same as those of the $e$ + 3-jet channel; thus, the jet efficiencies of the SM backgrounds are exactly the same. The more massive the Higgs, the larger the jet efficiencies are, as it is evident from Table VI.

(B) We required no presence of an electron in our event. If we find an electron with $p_T > 15.0$ GeV and $\eta < 3.0$, we reject such events, i.e., we are vetoing them. This selection largely reduced the SM back-

TABLE VI.    Same as in the previous table but for $\not{E}_T + 3$-jet channel. In the final column, we mention the significance ($\mathcal{S}$) defined as $\mathcal{S} = S/\sqrt{B}$, where $S(B)$ for signal (background) events for 100 fb$^{-1}$ of data after all cuts mentioned in the "I" column are implemented. The significances for 1000 fb$^{-1}$ are shown in parentheses.

| Proc, $m_h$ | RawEvt | A | B | C | D | E | F | G | H | I | $\mathcal{S}$ |
|---|---|---|---|---|---|---|---|---|---|---|---|
| $\nu-1, 65.93$ | 4114.1 | 1540.7 | 1475.6 | 200.6 | 112.5 | 111.2 | 102.0 | 49.8 | 47.8 | 26.0 | 3.34(10.6) |
| $\nu bbj$ | 213 85.4 | 4040.5 | 3928.5 | 244.7 | 43.0 | 33.1 | 32.1 | 5.3 | 5.2 | 4.1 | B = 60.5 |
| $\nu bjj$ | 4077.8 | 985.1 | 971.8 | 16.4 | 4.6 | 3.0 | 2.8 | 0.1 | 0.1 | 0.0 | |
| $\nu tb$ | 843 95.2 | 512 27.5 | 473 79.2 | 3671.2 | 709.1 | 661.3 | 598.4 | 27.7 | 26.3 | 12.5 | |
| $\nu jjj$ | 387 092 0.0 | 718 974.7 | 717 299.2 | 722.2 | 173.3 | 144.4 | 144.4 | 28.9 | 28.9 | 28.9 | |
| $ebbj$ | 268 839 0.0 | 176 148.3 | 407 28.9 | 5302.1 | 1389.0 | 1254.6 | 507.8 | 149.4 | 104.5 | 14.9 | |
| $ebjj$ | 330 834.0 | 313 17.5 | 7935.9 | 214.2 | 58.7 | 34.7 | 11.6 | 0.8 | 0.8 | 0.0 | |
| $et\bar{t}$ | 1425.5 | 1313.8 | 176.9 | 21.7 | 3.0 | 3.0 | 2.5 | 0.1 | 0.1 | 0.1 | |
| $ejjj$ | 372 241 00.0 | 494 304 9.0 | 100 295 1.5 | 3706.3 | 644.6 | 644.6 | 0.0 | 0.0 | 0.0 | 0.0 | |
| $\nu-2, 71.32$ | 2323.5 | 917.2 | 879.1 | 123.5 | 61.4 | 60.9 | 55.8 | 27.3 | 26.1 | 14.2 | 1.84(5.8) |
| $\nu bbj$ | 213 85.4 | 4040.5 | 3928.5 | 244.7 | 35.9 | 28.2 | 27.2 | 4.5 | 4.5 | 3.5 | B = 59.7 |
| $\nu bjj$ | 4077.8 | 985.1 | 971.8 | 16.4 | 4.3 | 2.9 | 2.6 | 0.1 | 0.1 | 0.0 | |
| $\nu tb$ | 843 95.2 | 512 27.5 | 473 79.2 | 3671.2 | 727.0 | 681.4 | 626.0 | 31.8 | 30.4 | 17.3 | |
| $\nu jjj$ | 387 092 0.0 | 718 974.7 | 717 299.2 | 722.2 | 202.2 | 173.3 | 173.3 | 28.9 | 28.9 | 28.9 | |
| $ebbj$ | 268 839 0.0 | 176 148.3 | 407 28.9 | 5302.1 | 1344.2 | 1209.8 | 433.1 | 89.6 | 59.7 | 0.0 | |
| $ebjj$ | 330 834.0 | 313 17.5 | 7935.9 | 214.2 | 59.5 | 36.4 | 15.7 | 0.8 | 0.8 | 0.0 | |
| $et\bar{t}$ | 1425.5 | 1313.8 | 176.9 | 21.7 | 3.3 | 3.3 | 2.8 | 0.1 | 0.1 | 0.0 | |
| $ejjj$ | 372 241 00.0 | 494 304 9.0 | 100 295 1.5 | 3706.3 | 483.4 | 322.3 | 0.0 | 0.0 | 0.0 | 0.0 | |
| $\nu-3, 83.77$ | 1830.6 | 845.3 | 809.8 | 116.0 | 44.0 | 43.4 | 40.0 | 21.2 | 20.7 | 11.1 | 1.54(4.9) |
| $\nu bbj$ | 213 85.4 | 4040.5 | 3928.5 | 244.7 | 24.2 | 20.0 | 19.5 | 3.8 | 3.8 | 3.0 | B = 52.1 |
| $\nu bjj$ | 4077.8 | 985.1 | 971.8 | 16.4 | 3.2 | 2.2 | 2.0 | 0.1 | 0.1 | 0.1 | |
| $\nu tb$ | 843 95.2 | 512 27.5 | 473 79.2 | 3671.2 | 736.0 | 695.9 | 643.3 | 36.0 | 35.3 | 20.1 | |
| $\nu jjj$ | 387 092 0.0 | 718 974.7 | 717 299.2 | 722.2 | 202.2 | 173.3 | 173.3 | 28.9 | 28.9 | 28.9 | |
| $ebbj$ | 268 839 0.0 | 176 148.3 | 407 28.9 | 5302.1 | 1015.6 | 896.1 | 388.3 | 104.5 | 74.7 | 0.0 | |
| $ebjj$ | 330 834.0 | 313 17.5 | 7935.9 | 214.2 | 38.9 | 25.6 | 13.2 | 0.0 | 0.0 | 0.0 | |
| $et\bar{t}$ | 1425.5 | 1313.8 | 176.9 | 21.7 | 3.6 | 3.6 | 2.9 | 0.2 | 0.2 | 0.0 | |
| $ejjj$ | 372 241 00.0 | 494 304 9.0 | 100 295 1.5 | 3706.3 | 322.3 | 0.0 | 0.0 | 0.0 | 0.0 | 0.0 | |
| $\nu-4, 88.07$ | 2018.0 | 975.7 | 932.1 | 133.8 | 47.0 | 46.5 | 42.8 | 23.9 | 23.5 | 12.6 | 1.75(5.5) |
| $\nu bbj$ | 213 85.4 | 4040.5 | 3928.5 | 244.7 | 22.0 | 18.3 | 18.0 | 3.6 | 3.6 | 2.8 | B = 52.0 |
| $\nu bjj$ | 4077.8 | 985.1 | 971.8 | 16.4 | 3.0 | 2.0 | 1.9 | 0.1 | 0.1 | 0.1 | |
| $\nu tb$ | 843 95.2 | 512 27.5 | 473 79.2 | 3671.2 | 720.1 | 680.0 | 624.7 | 34.6 | 33.2 | 20.1 | |
| $\nu jjj$ | 387 092 0.0 | 718 974.7 | 717 299.2 | 722.2 | 144.4 | 115.5 | 115.5 | 28.9 | 28.9 | 28.9 | |
| $ebbj$ | 268 839 0.0 | 176 148.3 | 407 28.9 | 5302.1 | 970.8 | 866.3 | 403.3 | 104.5 | 74.7 | 0.0 | |
| $ebjj$ | 330 834.0 | 313 17.5 | 7935.9 | 214.2 | 41.4 | 28.1 | 16.5 | 0.8 | 0.8 | 0.0 | |
| $et\bar{t}$ | 1425.5 | 1313.8 | 176.9 | 21.7 | 3.8 | 3.8 | 3.0 | 0.2 | 0.2 | 0.1 | |
| $ejjj$ | 372 241 00.0 | 494 304 9.0 | 100 295 1.5 | 3706.3 | 161.1 | 0.0 | 0.0 | 0.0 | 0.0 | 0.0 | |
| $\nu-5, 100.47$ | 1125.0 | 613.9 | 585.0 | 88.2 | 23.5 | 23.3 | 21.5 | 12.0 | 11.9 | 6.1 | 1.41(4.5) |
| $\nu bbj$ | 213 85.4 | 4040.5 | 3928.5 | 244.7 | 15.0 | 11.8 | 11.6 | 2.4 | 2.4 | 1.9 | B = 18.7 |
| $\nu bjj$ | 4077.8 | 985.1 | 971.8 | 16.4 | 1.9 | 1.3 | 1.3 | 0.1 | 0.1 | 0.1 | |
| $\nu tb$ | 843 95.2 | 512 27.5 | 473 79.2 | 3671.2 | 644.0 | 615.0 | 562.4 | 39.4 | 38.7 | 16.6 | |
| $\nu jjj$ | 387 092 0.0 | 718 974.7 | 717 299.2 | 722.2 | 115.5 | 86.7 | 86.7 | 28.9 | 28.9 | 0.0 | |
| $ebbj$ | 268 839 0.0 | 176 148.3 | 407 28.9 | 5302.1 | 806.5 | 672.1 | 313.6 | 59.7 | 29.9 | 0.0 | |
| $ebjj$ | 330 834.0 | 313 17.5 | 7935.9 | 214.2 | 25.6 | 17.4 | 11.6 | 2.5 | 2.5 | 0.0 | |
| $et\bar{t}$ | 1425.5 | 1313.8 | 176.9 | 21.7 | 4.0 | 3.9 | 3.0 | 0.2 | 0.2 | 0.1 | |
| $ejjj$ | 372 241 00.0 | 494 304 9.0 | 100 295 1.5 | 3706.3 | 483.4 | 322.3 | 0.0 | 0.0 | 0.0 | 0.0 | |

grounds as compared to the case with an explicit electron. For example, $ebbj$, $ebjj$, and $ejjj$ are reduced by approximately 77%, 75%, and 80%, while for $ett$ the reduction is close to 86.7%.

The $\nu jjj$, $\nu bjj$, and $\nu bbj$ are reduced by approximately 0.2%, 1.0%, and 3.0%, respectively. For the $\nu bbj$ case, having an secondary electron from *B*-meson semileptonic decay is more probable than in

$\nu bjj$ and much more probable than in $\nu jjj$. Such an expectation is, indeed, confirmed. The efficiencies of these selections for all of the five signal benchmarks are nearly identical (approximately 95.5%) as this is not related directly with the Higgs boson masses.

(C) Like in the $e + 3$-jet channel in the previous section, here we also demanded at least two $b$-tagged jets with the inclusion of a proper mistagging. The distributions of the number of $b$-tagged jets ($N_{b-tag}$) are shown in the right panel of Fig. 8. The efficiencies for the missing-energy signals and SM backgrounds are similar to the $e + 3$-jet channel, as the main difference between these two channels is the presence of an electron and missing energy.

(D) After identifying the $b$-tagged jet with proper mistagging, like in the leptonic channel, we follow the exact same procedure to reconstruct the non-SM Higgs boson ($m_{h_1}$) masses. The reconstructed di-$b$jet invariant mass, $m_{bb}$ tends to peak in the lower values rather than the benchmark values. Due to this, the mass window selection reduces the number of events more for a higher Higgs boson mass. As it is clear from Table VI, for the $\nu 1$–$\nu 5$ benchmarks cases the efficiencies are approximately 56.1%, 49.5%, 38.0%, 35.1%, and 26.6%. They are decreasing (as mentioned earlier) with the increase of the Higgs boson masses in the respective benchmark points. The $\nu bbj$ background survived by approximately 28.4%, 14.7%, 9.9%, 9.0%, and 6.1% for the $\nu 1$–$\nu 5$ benchmarks, respectively, follow a similar pattern like the signal benchmarks. We also find the same patterns for $ebbj$ background: 26.2%, 25.4%, 19.2%, 18.3%, and 15.2% (as the mass window selection depends upon the masses of the Higgs boson in the respective benchmarks). In addition, the $ebbj$ background has a Z-exchange diagram, i.e., $eZj$ with $Z \to b\bar{b}$. For the benchmark points where the Higgs boson is close to the Z-boson mass, i.e., for $\nu 4$ and $\nu 5$, the reduction is maximal. For $ebjj$, the events survived are approximately 27.4%, 27.7%, 18.1%, 19.3%, and 12.0% a for the $\nu 1$–$\nu 5$ benchmarks, respectively, somewhat similar to $ebbj$. For $ebjj$ two more issues are important to mention: the $ebZ$ with $Z \to j\bar{j}$ and mistagging of jets. For $\nu tb$, the events survived are approximately 19.0% for all the benchmark points, as many effects play together, e.g., top quark decay, mistagging, differences between Higgs boson, and W-boson masses in those benchmark points.

(E) Like in the electron channel selection (e), here we also demanded the presence of one forward jet. All the signal benchmarks survived by approximately

99%. This criterion has a mild overall impact: it rejects the irreducible backgrounds $\nu bbj$ ($\nu bjj$) by approximately 34.5%, 21.0%, 17.4%, 16.7%, and 21.7% (22.9%, 33.0%, 33.4%, 33.4%, and 29.0%) for the $\nu 1$–$\nu 5$ benchmarks, respectively. The background $\nu jjj$ is reduced by approximately 16.0%–25.0% from the $\nu 1$ to $\nu 5$ benchmark points.

(F) The signal now contains a neutrino, and this explicitly leads to missing energy (other than the jet-energy smearing and mismeasurements). The $\not{E}_T$ is shown in the right panel of Fig. 9. We demanded that $\not{E}_T$ should be larger than 15 GeV. All the signal benchmarks survived by 91% or more. These criteria suppressed all the background except for $ett$. Most importantly, at this stage $ejjj$ turns out to be zero. The $ebjj$ is reduced by 65%–35%, while $ebbj$ is reduced by 65%–55% for all of the signal benchmarks. The relatively larger reduction in $ebbj$ is again due to the semileptonic decays of the two bottom quarks. The background $\nu bbj$ survived by 99% for the $\nu 1$ benchmarks, and for all of the other benchmarks it survived by more than 96%, while $\nu bjj$ ($\nu jjj$) is survived by approximately 96% (99%).

(G) With the identification of the forward jet we reconstructed the three-jet invariant mass of the $m_{bbj_f}$. The distribution is shown in Fig. 13 for the $\nu 5$ benchmark. All other benchmarks have similar distributions, with the peaks at nearly the same values around 120 GeV. Furthermore, we demanded that the $m_{bbj_f} > 210$ GeV. The signal reduces by approximately 50% to 45% (from the $\nu 1$ to $\nu 5$ benchmark points) while the background reduces severely; e.g., $\nu bbj$ reduces by approximately 80%. The other irreducible backgrounds, $\nu tb$, $ebbj$, and $ett$ reduce by approximately 95%, 70%–80% and 96%–93%, respectively, for all of the signal benchmarks.

(H) Like in the $e + 3$-jet channel, we demanded $H_T > 100$ GeV. The event efficiencies for the signal and all backgrounds follow a similar pattern as the lepton signal channel. This is due to the fact that this variable depends on the number of jets and their transverse momenta and does not have an explicit dependence on either the electron or the neutrino. Except for $ebbj$ (reduced by approximately 30%), this selection hardly affects any other backgrounds.

At this stage, for all the signal benchmarks, the backgrounds of $\nu tb$ and $\nu jjj$ are of similar size to the signal events, while $ebbj$ is slightly more than a factor of two. The signal events are quite large, and the SM backgrounds are manageable. This leads to quite high significances to observe the Higgs boson signal in the missing energy channel.

(I)  However, to reduce the $ebbj$ further, we invoked the magnitude of $|\vec{H}_T| > 50$ GeV. The signals and the $\nu tb$ are reduced by approximately 50%, while $ebbj$ (except for the $\nu 1$ benchmark, where it was reduced by 85%) goes to zero.

After applying the cumulative selections from (A)–(I), we estimated the total SM background events to be found in the final column of Table VI. The significances for 100 $fb^{-1}$ integrated luminosity for the $\nu 1$, $\nu 2$, $\nu 3$, $\nu 4$, and $\nu 5$ benchmark points are $3.3\sigma$, $1.8\sigma$, $1.5\sigma$, $1.8\sigma$, and $1.4\sigma$, respectively. Thus, except for the first benchmark, with Higgs boson mass around 66.0 GeV, all other benchmarks are not good enough to be observed with a high confidence level with 100 $fb^{-1}$. We find that with 1000 $fb^{-1}$, the significances of those benchmarks can be found with $10.6\sigma$, $5.8\sigma$, $4.9\sigma$, $5.5\sigma$, and $4.5\sigma$. With our choices of simple cut-based selections and at the end of the LHeC, a $5.0\sigma$ discovery would be possible for Higgs boson masses up to 90 GeV.

Compared to the electron channel, the overall significances in the missing energy channel are higher for relatively large Higgs masses. However, likewise in the electron channel, here we have exploited the optimization by varying four different kinematical parameters, $\not{E}_T$, $m_{\phi j}$, $H_T$, and the magnitude of $\vec{H}_T$. The optimization starts after the events have passed the forward jet criteria (after selection criterion E). The numerical values of all these kinematical variables are varied within a maximum and minimum range (by seeing the corresponding distributions). We varied the $\not{E}_T$ in the ranges (10.0,40.0) with step size 5.0, together with $m_{\phi j}$, $H_T$, and the magnitude of $\vec{H}_T$ used in the electron channel with the same ranges. We have checked approximately 2464 combinations and estimated the number of signal events and the total SM backgrounds and, finally, the significances. The kinematical configurations and their numerical values for which the significances (in the fifth and ninth columns) for 100 fb$^{-1}$ are maximum is shown in Table VII. It turns out that one can have $2.4\sigma$ up to Higgs boson masses of 88 GeV. The significances in the parenthesis are for 1000 fb$^{-1}$. It turns out that the Higgs boson with masses more than 90 can have significances approximately $5\sigma$.

## V. CONCLUSIONS

The discovery of the SM-like Higgs boson at LHC establishes the correct pattern of the electroweak symmetry breaking with a doublet. However, to overcome theoretical shortcomings, multiple doublets are naturally introduced in models beyond the SM—both without and with supersymmetry. All such multiple doublet models predict the presence of more Higgses with different mass ranges. Hence, looking for any kind of such Higgses in the present and upcoming collision experiments is a good opportunity to probe particle physics beyond the SM.

Among the experimental facilities, which will soon become operational and potentially competitive to look for the intermediate mass Higgs bosons, is the LHeC facility (with $ep$ collisions) located at CERN expected to be operational in 2020.

In this work, we have considered the NMSSM model where the non-SM type Higgs boson with masses less than the SM-like Higgs boson is naturally possible with all the theoretical and most up-to-date experimental constraints from the low energy experiments as well as the supersymmetry and Higgs search results from the LHC. The model has a naturally low mass lightest neutralino ($\tilde{\chi}_1^0$) which serves as a possible candidate of the cold-dark matter. Apart from the particle physics constraints mentioned above, our parameter space respects all the dark matter constraints, including WMAP and dark matter searches.

We have considered two different production mechanisms of this intermediate Higgs boson, namely, $eh_1 q_f$ and $\nu h_1 q_f$, and used the $h_1 \to b\bar{b}$ decay mode to find the Higgs boson signal. In our analysis, we performed a detailed parameter space scanning using NMSSMTOOLS v.5.0.1, assuming that the second intermediate mass Higgs boson is of the SM type. For the allowed parameters, we estimated the production cross section and the branching ratio to find the event rate at the LHeC facility.

The production processes under consideration are $e$ + 3-jets and $\not{E}_T$ + 3-jets. Two jets can originate from the Higgs boson decay, $h_1 \to b\bar{b}$, and we demanded both of them to be $b$-tagged (with proper mistagging from light-flavor and gluon jets) in the central rapidity region. The remaining jet originates from the remnant of the proton fluxes which is

TABLE VII. The optimization of the signal channel with different sets of selection cuts, e.g., $\not{E}_T$, $m_{\phi j}$, $H_T$, the magnitude of $\vec{H}_T$ (see text for details) with the best significance obtained for 100 fb$^{-1}$. The significances in the parentheses are for 1000 fb$^{-1}$.

| BP, $m_h$ | $\not{E}_T, m_{\phi j}, H_T, \vec{H}_T$ | S | B | $\mathcal{S}$ | $\not{E}_T, m_{\phi j}, H_T, \vec{H}_T$ | S | B | $\mathcal{S}$ |
|---|---|---|---|---|---|---|---|---|
| $\nu 1, 65.93$ | 35 180 70 30 | 44.9 | 90.7 | 4.7(14.9) | 10 170 70 60 | 28.6 | 63.9 | 3.57(11.4) |
| $\nu 2, 71.32$ | 35 180 70 30 | 25.3 | 83.2 | 2.8(8.9) | 40 170 70 50 | 19.6 | 75.7 | 2.3(7.2) |
| $\nu 3, 83.77$ | 30 180 70 30 | 20.1 | 97.4 | 2.0(6.5) | 30 180 90 30 | 19.9 | 96.7 | 2.0(6.5) |
| $\nu 4, 88.07$ | 30 180 90 30 | 23.5 | 97.6 | 2.4(7.6) | 35 180 120 30 | 19.6 | 92.3 | 2.0(6.5) |
| $\nu 5, 100.47$ | 30 180 100 30 | 12.3 | 105.8 | 1.2(3.8) | 25 180 100 50 | 7.9 | 45.0 | 1.2(3.7) |

likely to be with large rapidity (in the forward or backward regions). We considered the reducible and irreducible SM backgrounds (with charge conjugation wherever appropriate) for the charge-current processes: $\nu tb$, $\nu bbj$, $\nu bjj$, and $\nu jjj$ and neutral current processes: $ebbj$, $ebjj$, $ett$, and $ejjj$.

We performed a full hadron–level Monte Carlo simulation using MADGRAPH/MADEVENT followed by PYTHIA as the parton shower/hadronization event generator and its PYCELL toy calorimeter in accordance with the LHeC detector parameters. We carefully implemented $b$-tagging, including mistagging of $c$-jets, light-flavor, and gluon jets.

In both of the Higgs signals under consideration, we first applied the basic event characteristics, like the number of jets, the number of leptons, the missing energy profile, and the number of $b$-tagged jets. The kinematics for both of the signals are very interesting due to the fact that the Higgs boson is produced in the central rapidity region such that the two $b$-tagged jets are also central. We reconstructed the invariant mass of these two (or more) $b$-tagged jets and identified the best combinations, where the reconstructed Higgs boson mass is close to the benchmark values and, thereafter, selected only events with slightly asymmetric choices with $m_{h_1} - 15 < m_{bb} < m_{h_1} + 5$ GeV. This selection reduces the SM backgrounds to a large extent and the invariant mass ensures the finding of the Higgs boson.

As the next step of our selection, by seeing the rapidity profiles, we identified the most energetic light-flavor forward jet ($j_f$) and demanded that the rapidity product of the forward lepton, i.e., electron ($j_e$) and forward jet should be negative; i.e., they must lie in the opposite hemisphere. Furthermore, we demanded that the rapidity gap between this forward jet and forward electron should satisfy $-5.5 < \Delta\eta_{jf-ef} < 0.5$. After this selection we calculated the three-jet invariant masses, $m_{bbj_f}$, which essentially gives the overall energy scale of the hard scattering. We demanded that this should be larger than 190 GeV, and this selection helps to suppress backgrounds coming from $ebbj$, $ejjj$, $\nu tb$, and $ett$.

After that, for the $e + 3j$ signal channel, we applied some $H_T$ selections to suppress the SM backgrounds further. This is not enough, though, to ensure a relatively high confidence level. Hence, finally, we exploited the $\vec{H}_T$ which leads to better significances, but not at the discovery level, though, for the intermediate non-SM type Higgs boson.

In the $e + 3j$ channel, which is naturally event rate limited, we found that to isolate the non-SM like Higgs signals, we can attain at most $0.4\sigma$ with 100 $fb^{-1}$ for the $e1$ benchmark. With ten times more luminosity, for the same

benchmark with $m_h = 63.59$ GeV, we would have the significance of approximately $1.3\sigma$.

In the $\not{E}_T + 3j$ channel with a large event rate, we can probe a much higher Higgs mass. We find that with 100 $fb^{-1}$ for the $\nu 1$ benchmark, the significance would be approximately $3.3\sigma$. For the $\nu 4$ benchmark (same as the $e5$ benchmark), we can have the significance of approximately $1.8\sigma$. With 1000 $fb^{-1}$ for the $\nu 4$ benchmark, with Higgs masses 88.1 GeV, we would have $5.5\sigma$. And for the $\nu 5$ benchmark, with Higgs masses of 100.5 GeV, we found the significance of $4.5\sigma$. Using a mere interpolation, we would expect that one can have $5.0\sigma$ significance up to the Higgs masses of around 90 GeV.

It should be noted that we have adopted a simple cut-based selection. If one would instead invoke more complex discriminators and/or use multivariate analysis, we expect that the significance would be larger even with the low-luminosity option.

We have introduced a simple cut-based optimization method to enhance the Higgs boson mass reach in both the channels under consideration. In the electron channel, by varying the most important kinematical variables, $\eta_l$, $\Delta\eta_{jl}$, $m_{\phi j}$, $H_T$, and the magnitude of $\vec{H}_T$ with the maximum and minimum ranges (by inspecting the respective distributions), we optimized the significances. We found that for 100 (1000) $fb^{-1}$ integrated luminosity, we can have the significances of $2.1\sigma$ ($6.6\sigma$) for the $e4$ benchmark point with the Higgs boson masses of 82.2 GeV.

In the missing energy channel, by varying $\not{E}_T$, $m_{\phi j}$, $H_T$, and magnitude of $\vec{H}_T$, for 100 $fb^{-1}$ integrated luminosity, we can have the significances of $2.4\sigma$ ($1.2\sigma$) for the $\nu 4$ ($\nu 5$) benchmark point with Higgs boson masses of 88.1 (100.5) GeV. With the high luminosity option, one would expect the $5\sigma$ discovery, at least up to Higgs boson masses of 95 GeV.

To conclude, after the first few years of the LHeC run, and using more complex discriminators and using multivariate analyses, we expect that in the $e + 3j$ channel, non-SM type Higgs bosons would be probed up to 85–90 GeV. In the $\not{E}_T + 3j$, one can extend the reach at least up to 95 GeV.

[1] G. Aad *et al.* (ATLAS Collaboration), Phys. Lett. B **716**, 1 (2012).

[2] S. Chatrchyan *et al.* (CMS Collaboration), Phys. Lett. B **716**, 30 (2012).

[3] J. D. Wells, arXiv:0909.4541; I. P. Ivanov, Prog. Part. Nucl. Phys. **95**, 160 (2017).

[4] C. Grojean, Report No. CERN-PH-TH-2006-172.

[5] P. S. Bhupal Dev, C. H. Lee, and R. N. Mohapatra, J. Phys. Conf. Ser. **631**, 012007 (2015).

[6] G. Seidl, arXiv:hep-ph/0409162; C. Csaki, arXiv:hep-ph/0412339.

[7] G. C. Branco, P. M. Ferreira, L. Lavoura, M. N. Rebelo, M. Sher, and J. P. Silva, Phys. Rep. **516**, 1 (2012).

[8] J. F. Gunion and H. E. Haber, Phys. Rev. D **67**, 075019 (2003).

[9] A. Cordero-Cid, J. Hernandez-Sanchez, C. G. Honorato, S. Moretti, M. A. Perez, and A. Rosado, J. High Energy Phys. 07 (2014) 057; O. Felix-Beltran, F. Gonzalez-Canales, J. Hernandez-Sanchez, S. Moretti, R. Noriega-Papaqui, and A. Rosado, Phys. Lett. B **742**, 347 (2015); J. Hernandez-Sanchez, S. Moretti, R. Noriega-Papaqui, and A. Rosado, J. High Energy Phys. 07 (2013) 044; *Proc. Sci.*, CHARGED (2012) 029; J. Hernandez-Sanchez, C. G. Honorato, M. A. Perez, and J. J. Toscano, Phys. Rev. D **85**, 015020 (2012); J. L. Diaz-Cruz and J. J. Toscano, Phys. Rev. D **62**, 116005 (2000); A. G. Akeroyd, S. Moretti, and J. Hernandez-Sanchez, *Proc. Sci.*, CHARGED (2014) 025.

[10] G. L. Kane, C. F. Kolda, L. Roszkowski, and J. D. Wells, Phys. Rev. D **49**, 6173 (1994).

[11] H.-P. Nilles, M. Srednicki, and D. Wyler, Phys. Lett. **120B**, 346 (1983); J. P. Derendinger and C. A. Savoy, Nucl. Phys. **B237**, 307 (1984); J. R. Ellis, J. F. Gunion, H. E. Haber, L. Roszkowski, and F. Zwirner, Phys. Rev. D **39**, 844 (1989); U. Ellwanger, Phys. Lett. B **303**, 271 (1993).

[12] M. Drees, Int. J. Mod. Phys. A **04**, 3635 (1989).

[13] F. Franke and H. Fraas, Int. J. Mod. Phys. A **12**, 479 (1997).

[14] M. Maniatis, Int. J. Mod. Phys. A **25**, 3505 (2010).

[15] U. Ellwanger, C. Hugonie, and A. M. Teixeira, Phys. Rep. **496**, 1 (2010).

[16] P. Diessner, J. Kalinowski, W. Kotlarski, and D. Stoeckinger, J. High Energy Phys. 03 (2016) 007.

[17] K. Hagimoto, T. Kobayashi, H. Makino, K. i. Okumura, and T. Shimomura, J. High Energy Phys. 02 (2016) 089.

[18] D. J. Miller, S. Moretti, and R. Nevzorov, arXiv:hep-ph/0501139.

[19] R. Barbieri, D. Buttazzo, K. Kannike, F. Sala, and A. Tesi, Phys. Rev. D **87**, 115018 (2013); M. Farina, M. Perelstein, and B. Shakya, J. High Energy Phys. 04 (2014) 108.

[20] J. E. Kim and H. P. Nilles, Phys. Lett. **138B**, 150 (1984).

[21] J. R. Ellis, J. F. Gunion, H. E. Haber, L. Roszkowski, and F. Zwirner, Phys. Rev. D **39**, 844 (1989).

[22] For e.g., P. Bechtle, H. E. Haber, S. Heinemeyer, O. Stl, T. Stefaniak, G. Weiglein, and L. Zeune, Eur. Phys. J. C **77**, 67 (2017); J. Quevillon, arXiv:1405.2241; B. Dumont, J. F. Gunion, and S. Kraml, Phys. Rev. D **89**, 055018 (2014).

[23] P. Drechsel, L. Galeta, S. Heinemeyer, and G. Weiglein, Eur. Phys. J. C **77**, 42 (2017); P. Drechsel, Report No. DESY-THESIS-2016-019; F. Staub, P. Athron, U. Ellwanger, R. Grober, M. Muhlleitner, P. Slavich, and A. Voigt, Comput. Phys. Commun. **202**, 113 (2016).

[24] M. D. Goodsell and F. Staub, Eur. Phys. J. C **77**, 46 (2017).

[25] U. Ellwanger, J. F. Gunion, C. Hugonie, and S. Moretti, arXiv:hep-ph/0401228; V. Barger, P. Langacker, H. S. Lee, and G. Shaughnessy, Phys. Rev. D **73**, 115010 (2006); D. J. Miller, R. Nevzorov, and P. M. Zerwas, Nucl. Phys. **B681**, 3 (2004); U. Ellwanger and M. Rodriguez-Vazquez, J. High Energy Phys. 02 (2016) 096; J. S. Kim, D. Schmeier, and J. Tattersall, Phys. Rev. D **93**, 055018 (2016); J. Rathsman and T. Rossler, Adv. High Energy Phys. **2012**, 853706 (2012); R. Enberg, R. Pasechnik, and O. Stal, Phys. Rev. D **85**, 075016 (2012); J. F. Gunion, Y. Jiang, and S. Kraml, Phys. Lett. B **710**, 454 (2012); S. Liebler, H. Mantler, and M. Wiesemann, arXiv:1608.02949; M. Carena, H. E. Haber, I. Low, N. R. Shah, and C. E. M. Wagner, Phys. Rev. D **93**, 035013 (2016); E. Conte, B. Fuks, J. Guo, J. Li, and A. G. Williams, J. High Energy Phys. 05 (2016) 100; S. F. King, M. Muhlleitner, R. Nevzorov, and K. Walz, Nucl. Phys. **B870**, 323 (2013); S. F. King, M. Muhlleitner, and R. Nevzorov, Nucl. Phys. **B860**, 207 (2012); N. D. Christensen, T. Han, Z. Liu, and S. Su, J. High Energy Phys. 08 (2013) 019; J. Cao, F. Ding, C. Han, J. M. Yang, and J. Zhu, J. High Energy Phys. 11 (2013) 018; G. Belanger, U. Ellwanger, J. F. Gunion, Y. Jiang, S. Kraml, and J. H. Schwarz, J. High Energy Phys. 01 (2013) 069; U. Ellwanger, J. F. Gunion, C. Hugonie, and S. Moretti, arXiv:hep-ph/0305109; D. Das, U. Ellwanger, and A. M. Teixeira, J. High Energy Phys. 04 (2012) 067; U. Ellwanger and C. Hugonie, Adv. High Energy Phys. **2012**, 625389 (2012); K. S. Jeong, Y. Shoji, and M. Yamaguchi, J. High Energy Phys. 11 (2014) 148; B. Dutta, Y. Gao, and B. Shakya, Phys. Rev. D **91**, 035016 (2015); S. Baum, K. Freese, N. R. Shah, and B. Shakya, Phys. Rev. D **95**, 115036 (2017).

[26] H. K. Dreiner, F. Staub, and A. Vicente, Phys. Rev. D **87**, 035009 (2013).

[27] U. Ellwanger, J. High Energy Phys. 11 (2013) 108.

[28] F. Domingo and G. Weiglein, J. High Energy Phys. 04 (2016) 095.

[29] D. Barducci, G. Belanger, C. Hugonie, and A. Pukhov, J. High Energy Phys. 01 (2016) 050.

[30] N. E. Bomark, S. Moretti, S. Munir, and L. Roszkowski, *Proc. Sci.*, EPS-HEP2015 (2015) 162; *J. High Energy Phys.* 02 (2015) 044; S. Moretti and S. Munir, Adv. High Energy Phys. **2015**, 509847 (2015); M. M. Almarashi and S. Moretti, Phys. Rev. D **85**, 017701 (2012); **84**, 015014 (2011); N. E. Bomark, S. Moretti, S. Munir, and L. Roszkowski, *Proc. Sci.*, CHARGED (2014) 029; N. E. Bomark, S. Moretti, and L. Roszkowski, J. Phys. G **43**, 105003 (2016); M. M. Almarashi and S. Moretti, Phys. Rev. D **83**, 035023 (2011).

[31] C. T. Potter, Eur. Phys. J. C **76**, 44 (2016).

[32] M. Guchait and J. Kumar, Int. J. Mod. Phys. A **31**, 1650069 (2016); M. Guchait and J. Kumar, Phys. Rev. D **95**, 035036 (2017).

[33] V. Khachatryan *et al.* (CMS Collaboration), J. High Energy Phys. 01 (2016) 079.

[34] https://lhec.web.cern.ch.

[35] See for e.g., M. Klein and R. Yoshida, Prog. Part. Nucl. Phys. **61**, 343 (2008).

[36] T. Han and B. Mellado, Phys. Rev. D **82**, 016009 (2010).

[37] I. A. Sarmiento-Alvarado, A. O. Bouzas, and F. Larios, J. Phys. G 42, 085001 (2015); A. O. Bouzas and F. Larios, J. Phys. Conf. Ser. 651, 012004 (2015).

[38] S. P. Das, J. Hernandez-Sanchez, S. Moretti, A. Rosado, and R. Xoxocotzi, Phys. Rev. D 94, 055003 (2016).

[39] M. Drees and G. Gerbier, arXiv:1204.2373.

[40] J. C. Sanabria, Revista de la Academia colombiana de ciencias exactas, fisicas y naturales : (publicacion del Ministerio de educacion nacional) 38, 34 (2014).

[41] P. Ade et al. (Planck Collaboration), Astron. Astrophys. 594, A13 (2016).

[42] G. Belanger, F. Boudjema, C. Hugonie, A. Pukhov, and A. Semenov, J. Cosmol. Astropart. Phys. 09 (2005) 001; J. Cao, Y. He, L. Shang, W. Su, P. Wu, and Y. Zhang, J. High Energy Phys. 10 (2016) 136; J. Cao, Y. He, L. Shang, W. Su, and Y. Zhang, J. High Energy Phys. 08 (2016) 037; D. Das and U. Ellwanger, J. High Energy Phys. 09 (2010) 085; Q. F. Xiang, X. J. Bi, P. F. Yin, and Z. H. Yu, Phys. Rev. D 94, 055031 (2016); J. Kozaczuk and S. Profumo, Phys. Rev. D 89, 095012 (2014).

[43] M. Badziak, M. Olechowski, and P. Szczerbiak, J. High Energy Phys. 03 (2016) 179.

[44] S. Horiuchi, O. Macias, D. Restrepo, A. Rivera, O. Zapata, and H. Silverwood, J. Cosmol. Astropart. Phys. 03 (2016) 048.

[45] J. D. Ruiz-Alvarez, C. A. de S.Pires, F. S. Queiroz, D. Restrepo, and P. S. Rodrigues da Silva, Phys. Rev. D 86, 075011 (2012).

[46] S. P. Das, M. Guchait, and D. P. Roy, Phys. Rev. D 90, 055011 (2014).

[47] A. Florez, L. Bravo, A. Gurrola, C. Avila, M. Segura, P. Sheldon, and W. Johns, Phys. Rev. D 94, 073007 (2016).

[48] C.-C. Jean-Louis and G. Moreau, J. Phys. G 37, 105015 (2010).

[49] U. Ellwanger, J. F. Gunion, and C. Hugonie, J. High Energy Phys. 02 (2005) 066.

[50] S. Zheng, Eur. Phys. J. C 75, 195 (2015).

[51] D. Barducci, G. Belanger, J. Bernon, F. Boudjema, J. DaSilva, S. Kraml, U. Laa, and A. Pukhov, arXiv: 1606.03834.

[52] G. Belanger, F. Boudjema, A. Pukhov, and A. Semenov, Comput. Phys. Commun. 185, 960 (2014).

[53] J. C. Sanabria (ATLAS and CMS Collaborations), Nucl. Part. Phys. Proc. 267, 25 (2015).

[54] G. Aad et al. (ATLAS and CMS Collaborations), J. High Energy Phys. 08 (2016) 045.

[55] V. Khachatryan et al. (CMS Collaboration), J. High Energy Phys. 02 (2017) 135.

[56] G. Aad et al. (ATLAS Collaboration), J. High Energy Phys. 11 (2015) 206.

[57] A. Butter, T. Plehn, M. Rauch, D. Zerwas, S. Henrot-Versill, and R. Lafaye, Phys. Rev. D 93, 015011 (2016).

[58] S. Schael et al. (SLD Electroweak Group, DELPHI, ALEPH, SLD, SLD Heavy Flavour Group, OPAL, LEP Electroweak Working Group, and L3 Collaborations), Phys. Rep. 427, 257 (2006).

[59] G. W. Bennett et al. (Muon g-2 Collaboration), Phys. Rev. Lett. 92, 161802 (2004).

[60] Y. Amhis et al. [Heavy Flavor Averaging Group (HFAG) Collaboration], arXiv:1412.7515.

[61] J. P. Lees et al. (BABAR Collaboration), Phys. Rev. D 88, 031102 (2013).

[62] M. Aaboud et al. (ATLAS Collaboration), Phys. Rev. D 94, 032005 (2016).

[63] J. Alwall, R. Frederix, S. Frixione, V. Hirschi, F. Maltoni, O. Mattelaer, H.-S. Shao, T. Stelzer, P. Torrielli, and M. Zaro, J. High Energy Phys. 07 (2014) 079.

[64] O. Bruening and M. Klein, Mod. Phys. Lett. A 28, 1330011 (2013).

[65] J. L. Abelleira Fernandez et al. (LHeC Study Group Collaboration), arXiv:1211.5102.

[66] J. L. Abelleira Fernandez et al. (LHeC Study Group Collaboration), J. Phys. G 39, 075001 (2012).

[67] See for e.g. R. B. Appleby, L. Thompson, B. Holzer, M. Fitterer, N. Bernard, and P. Kostka, J. Phys. G 40, 125004 (2013).

[68] R. D. Ball, V. Bertone, S. Carrazza, L. Del Debbio, S. Forte, A. Guffanti, N. P. Hartland, and J. Rojo (NNPDF Collaboration), Nucl. Phys. B877, 290 (2013); J. High Energy Phys. 04 (2015) 040.

[69] J. Pumplin, D. R. Stump, J. Huston, H. L. Lai, P. M. Nadolsky, and W. K. Tung, J. High Energy Phys. 07 (2002) 012.

[70] T. Sjostrand, S. Mrenna, and P. Z. Skands, J. High Energy Phys. 05 (2006) 026.

[71] R. N. Cahn and S. Dawson, Phys. Lett. B 136, 196 (1984); M. S. Chanowitz and M. K. Gaillard, Phys. Lett. B 142, 85 (1984); G. L. Kane, W. W. Repko, and W. B. Rolnick, Phys. Lett. B 148, 367 (1984).

[72] P. Agrawal, S. Bandyopadhyay, and S. P. Das, arXiv: 1308.6511.

[73] P. Agrawal, S. Bandyopadhyay, and S. P. Das, Phys. Rev. D 88, 093008 (2013).

[74] S. P. Das and M. Drees, Phys. Rev. D 83, 035003 (2011); J. Phys. Conf. Ser. 259, 012071 (2010); S. P. Das, A. Datta, and M. Drees, AIP Conf. Proc. 1078, 223 (2009).